Bulletin of the Seismological Society of America, Vol. 94, No. 6, pp. 2090–2109, December 2004

Ground-Motion Amplification in Nonlinear Soil Sites with Uncertain Properties

by Paolo Bazzurro* and C. Allin Cornell

Abstract This work presents a statistical study on the effect of soil layers with uncertain properties on ground-motion intensity at the soil surface. Surface motion is obtained by applying multiple real rock earthquake records at the base of different characterizations of the soil column, each one generated via Monte Carlo simulation. The effect of the soil is studied in terms of a site-specific, frequency-dependent amplification function, $AF(f)$, where f is a generic oscillator frequency. The goal here is the identification of ground-motion parameters that allow an efficient prediction of $AF(f)$. We investigated magnitude, M, source-to-site distance, R, of the input bedrock accelerogram along with bedrock ground-motion parameters such as peak ground acceleration, PGA_r, and spectral acceleration values, $S_a^r(f)$ and $S_a^r(f_{sc})$, both at the generic frequency f and at the specific initial fundamental frequency of vibration, f_{sc} of the soil column. This work includes two case studies: a saturated sandy site and a saturated soft clayey site. In the former, loss of shear strength owing to cyclic mobility is anticipated for severe levels of ground shaking, while in the latter, significant amplification is expected at long oscillator periods. The results show that $S_a^r(f)$ of the input record is the single most helpful parameter for the prediction of $AF(f)$ at the same oscillator frequency, f. $S_a^r(f)$ is more informative than PGA_r and/or the pair of M and R values of the event that generated the bedrock motion. A sufficiently accurate estimate of the median $AF(f)$ can be obtained by using 10 or fewer records, which may be selected without undue attention to the specific scenario events (i.e., M and R pairs) that control the hazard at the site. Finally, the effect of the uncertainty in the soil parameters on the prediction error of $AF(f)$ is of secondary importance compared to that from record-to-record variability. These findings will be used to estimate the hazard at the soil surface in a companion article in this issue (Bazzurro and Cornell, 2004).

Introduction

It has long been recognized that the severity and the frequency content of ground motions at a site are significantly dependent on the soil characteristics of the layers below the surface. At most sites, however, the soil profile and the parameters that control the soil dynamic response are not known with certainty. In this study we investigate from a probabilistic standpoint the effect of soil deposits with uncertain properties on surface ground shaking.

Many researchers have examined from several different perspectives the problem of site amplification of ground motions in a probabilistic framework (e.g., Faccioli, 1976; Whitman and Protonotarios, 1977; Costantino *et al.*, 1993; Silva, 1993, 1997a; Electric Power Research Institute, 1993; Hwang and Huo, 1994; Lee *et al.*, 1998; Tsai, 2000). This work, however, is fully probabilistic in that it includes the variability both in the input ground motion and in the soil parameters, and it is specifically aimed at an efficient prediction of the site amplification.

More precisely, the focus is on estimating the frequency-dependent nonlinear amplification (or transfer) function, $AF(f)$, of the spectral acceleration for a range of oscillator frequencies of interest for engineered structures. The term $AF(f)$ at the oscillator frequency, f, is defined here as the ratio of the spectral acceleration at the surface, $S_a^s(f)$, to the spectral acceleration at the bedrock, $S_a^r(f)$. To enable an accurate, yet effective, prediction of $AF(f)$ (i.e., involving the least possible number of soil-response analyses for the required accuracy) it is of paramount importance to identify one or more input ground-motion parameters that are well correlated with $AF(f)$ and, at the same time, that are themselves predictable. This statistical investigation is performed

*Present address: AIR Worldwide, San Francisco, California.

here via a comprehensive set of multiple-regression analyses of $AF(f)$ versus event parameters magnitude, M, source-to-site distance, R, and bedrock ground-motion parameters such as peak ground acceleration, PGA_r, and spectral-acceleration values, $S_a^r(f)$ and $S_a^r(f_{sc})$, one at the generic frequency, f, and the other at the initial fundamental frequency of vibration, f_{sc}, of the soil column.

The values of $AF(f)$, are obtained by driving a suite of real rock ground motions through different representations of the soil model. Each representation is characterized by a different but plausible combination of soil-parameter values selected by Monte Carlo simulation. To obtain a reliable estimate of the soil response, the analyses are performed in the time domain, using a nonlinear finite-element computer program capable of predicting the pore-water-pressure buildup and dissipation, SUMDES (Li *et al.*, 1992). From a purely probabilistic standpoint, however, any method of nonlinear soil response may be used instead, including equivalent-linear, frequency-domain-based methods such as the SHAKE program (Schnabel *et al.*, 1972).

Two actual offshore sites, one sandy and one clayey, are considered in this article. The sandy site is expected to show considerable nonlinear behavior owing to cyclic degradation during intense ground shaking, whereas the clayey site is anticipated to exhibit severe amplification of motion at low frequencies owing to soft-soil conditions. The results of this study show, quite surprisingly, that the amplification functions for these two sites possess consistent statistical characteristics in terms of dependence (or lack thereof) on parameters of the input ground motions and of the generating earthquakes.

Strong Ground Motion Database

The database of free-field surface rock strong ground motions (Table A1 in the Appendix) includes a total of 78 seismograms from 28 different earthquakes that occurred worldwide between 1966 and 1995 (Silva, 1997b). No special care was taken to discriminate near-source from far-field records. This large sample of records is adopted only to validate the results of this research, whereas, as discussed later, applications may need a much smaller suite of ground motions. The accelerograms are obtained from sites classified as "rock" sites according to at least one of the U.S. Geological Survey and Geomatrix classification schemes (for a review, see Abrahamson, 1996). The average shear-wave velocity, Vs_{30}, in the top 30 m (values that have become available to us after the main development of this study), however, indicate that some of these stations should have been more appropriately classified as stiff-soil sites. The somewhat mixed selection of stiff-soil and soft-rock records, however, does not invalidate the statistical findings that represent the main contribution of this study. Similar results were found by running the 47 out of 78 accelerograms in the databse that were recorded at stations with Vs_{30} greater than 500 m/sec.

Another issue regards the concentration (about 40%) of accelerograms that were recorded during three California earthquakes: the Loma Prieta (1989), Landers (1992), and Northridge (1994) events. This concentration, however, does not statistically affect the results of the regression analyses to follow. Little or no difference was found when 22 records from these three events were suppressed.

The range of M values is between $M5$ and $M7.4$, whereas the shortest distance values from the recording station to the ruptured area, R, range from 0 to 142 km (Fig. 1). As an aside, note that in the following regression analyses, instead of R we used $R_{\text{mod}} = \sqrt{R^2 + h^2}$, where the frequency-dependent values of h were taken from table 3 in Abrahamson and Silva (1997). R_{mod} has a slightly larger predictive power than R in predicting $AF(f)$ at short distances. This effect, however, is minor.

One horizontal component of each recording was chosen at random and used in the amplification study. The 5%-damped response spectra of all records, along with the mean and median spectra, are displayed in Figure 2. The selected accelerograms have PGA_r values ranging from about 0.01 g to 1.5 g. To ensure that the ground-motion signal is correct up to a period of at least 5 sec, only components corrected by using a high-pass frequency less than or equal to 0.2 Hz were selected. This issue may be important when a soil column undergoes cyclic degradation with a consequent increase in its effective vibration period.

Such accelerograms were applied directly at the base of the soil column without any prior deconvolution (e.g., Kramer, 1996). This assumption is believed to be valid up to a (site-dependent) frequency usually about 2 Hz, but it underestimates the motion at the column base above that threshold (Steidl *et al.*, 1996). The high-frequency de-amplification phenomenon is induced by near-surface weathering and cracking of the surface rock outcrop. It should be mentioned that a possible underestimation of the amplification at high frequencies is not crucial for the great majority of longer period structures (e.g., taller buildings, bridges, offshore platforms, etc.) that may warrant detailed soil-amplification studies like the one proposed here.

Deconvolution was not performed, because the main focus is more on showing the feasibility of the proposed procedure rather than on providing the best possible engineering estimate of $AF(f)$ at all frequencies for these two sites. If we were to use deconvolved accelerograms, only the amplitude of $AF(f)$ at some frequencies could conceivably be affected. We have no reason to expect that the statistical characteristics of $AF(f)$ would be any different. The unavoidable significant amount of subjective judgment that needs to be exercised when performing nonlinear deconvolution of accelerograms recorded at sites with poorly known characteristics would also have added a source of possible noise. Moreover, adding this delicate and time-consuming extra step would have shifted the bulk of our effort to an aspect of the problem of less direct interest here. In practical applications, however, when a much more limited number of

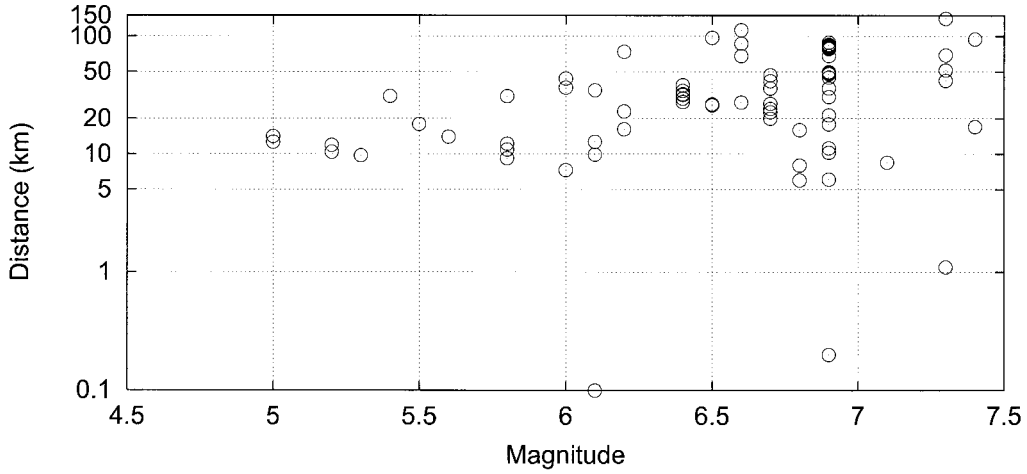

Figure 1. Scattergram of the M and R values included in the database.

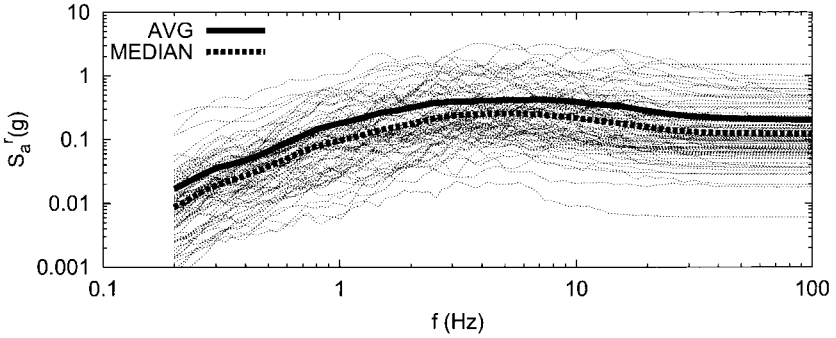

Figure 2. Response spectra at 5% of damping of the selected records.

accelerograms would most likely be used, deconvolution could be added as a preliminary step, if needed.

Note, however, that although deconvolution was not performed, the software used for soil-response computations modifies the recorded rock motion to obtain the motion at the rock–soil interface (i.e., the input motion at the base of the soil column). The rock base is modeled as a uniform elastic half-space with no damping. To satisfy the equilibrium and continuity conditions of the soil deposit and its underlying rock half-space, the stresses and displacements at the top of the half-space are equated to the stresses and displacements at the bottom of the soil deposit. This approach takes into account the variation of the seismic motion resulting from the presence of a soil deposit on top of the rock surface.

Response Software and Soil Modeling

Computer Program for Soil-Response Computation

The computer program adopted for assessing the soil-site response is SUMDES (Li *et al.*, 1992). This finite-element program is formulated on the basis of the effective-stress principle, vectored motion, transient pore-fluid movement, and generalized material stiffness. It is capable of predicting three-directional motions and the pore-pressure buildup and dissipation within soil deposits subjected to vertically propagating earthquake waves. Unlike the widely used SHAKE program (Schnabel *et al.*, 1972), which uses an equivalent-linear model, SUMDES can describe liquefaction or cyclic-mobility phenomena. Li *et al.* (1998) presents a case study where results from SUMDES compare well with data recorded during the 1986 Lotung earthquake in Taiwan.

The inelastic constitutive reduced-order bounding-surface model used in the analyses is a simplified version of the hypoplasticity model (Li *et al.*, 1992). As previously described, the boundary conditions (i.e., elastic base) were chosen to accommodate the rock-outcrop nature of the input.

SUMDES was modified by the authors (1) to run in cascade for multiple input records, (2) to modify for each layer (if requested by the user) the values assigned to a set of soil parameters according to specified probability distributions and correlation structure (see subsection to come for details), and (3) to yield additional output files that are ready for performing regression analyses. These modifications, however, do not affect the core of the program.

Description of the Sites

Both soil sites are located in the Mediterranean Sea.

The sandy deposit, which is under 45 m of water, consists of sands and gravels with sporadic cobbles. The relative

proportions of sand and gravel vary slightly at different depths within the zone. No cohesive or cemented strata were encountered during drilling. The relative density is between 60% and 80%, and the total unit weight is 20 kN/m^3. The behavior of this sand under undrained shear is dilative, and the effect of pore-pressure buildup and cyclic mobility can be relevant, depending on the amplitude of shear loading and the number of loading cycles. This effect tends to soften the soil by increasing the shear-strain level at which dilation occurs. The constitutive relationship adopted in SUMDES describes this phenomenon reasonably well. We recall, however, that the focus here is on predicting the spectral-acceleration amplification function, $AF(f)$, and not deformations within the soil deposit. Besides an improved constitutive model, a reliable computation of soil deformations would require 2D or 3D soil modeling. This aspect is not investigated in this study.

The clayey deposit, under 28 m of water, is cohesive (silts and clays) and soft, with both normally and overconsolidated layers. The shear modulus at small strain levels, $G_{\max}$, was established on the basis of both shear-wave velocity, V_s, measurements and correlations between the cone-tip resistance and V_s. The $G/G_{\max}$ versus shear-strain curves were obtained from Li *et al.* (1992).

In both cases, a soil column of 100 m was modeled by using 100 elements of 1 m of thickness each. For the clayey and the sandy sites, the median V_s increases from values at the mud line of 50 m/sec and 100 m/sec, respectively, to 400 m/sec at 100 m of depth. Although in both cases the bedrock is deeper than 100 m below the seabed, a taller soil column was not modeled because amplification at the surface is expected not to be significantly different for frequencies above the initial fundamental frequency of vibration, f_{sc}, of the soil column. For example, Ni *et al.* (1997, p. 354) state that for deep saturated deposits "the location of the rock where the base excitation is to be specified does not need to be known precisely in response studies." The same researchers observe that only the linear resonant frequency may be affected.

Also note that SUMDES carries out the soil-response computations in terms of effective stresses. The effective stresses in the soil mass (and therefore the soil strength and deformability) are not affected by the presence of the water overburden. Furthermore, no vertically propagating compression wave was considered in our analyses, and therefore the boundary conditions applied at the top boundary (i.e., zero shear and normal stresses) are appropriate.

Although the two columns considered here are fully saturated, it is important to stress that the statistical characteristics of the amplification function that constitute the main finding of this work apply also to soil formations onshore. We considered several other onshore soil columns, unsaturated or partially saturated with a wide variety of different soil properties (e.g., Pelli *et al.*, 2004). The response analyses of these columns yielded $AF(f)$s that were, of course, numerically different from one another and from those presented here. The statistical properties, however, were consistent with those shown in this article.

Soil Modeling

To estimate $AF(f)$, two different numerical characterizations of the soil column were used for each site: the *base case*, with deterministic soil properties whose values are equal to their best engineering estimates, and the *randomized case*, with uncertain soil properties. The purpose of this second model is to isolate the effect on $AF(f)$ deriving from the variability of the soil properties from the effect from record-to-record variability.

The values of the soil parameters were established by an extensive field- and laboratory-investigation program. The variability in the soil properties was included (in the randomized case) through a Monte Carlo approach by randomly varying the coefficient of permeability (π_0), the shear and the compression viscous damping ratios at 1 Hz (ξ_s and ξ_c), the coefficient of lateral Earth pressure at rest (K_0), the coefficient, G_0, which defines the elastic shear modulus $G_{\max}$ at very low strain levels, the friction angle, Φ_0, and the shear-strain value, $\gamma_{64\%}$, at 64% of $G/G_{\max}$. The same random perturbation factor is applied along the entire $G/G_{\max}$ versus γ curve.

The seven basic random variables (RVs) were considered lognormally distributed with $\sigma_{\ln \mathrm{RV}}$ equal to 0.25 for ξ_s, ξ_c, K_0, and G_0; to 0.1 for Φ_0; to 0.35 for $\gamma_{64\%}$, and to 0.7 for π_0. (Note that π_0 was held constant when characterizing the clayey site.) A distribution truncation at $\pm 2\sigma_{\ln \mathrm{RV}}$ was adopted to prevent unrealistic parameter values. An example of the scatter produced by the randomization is shown in Figure 3 for the sandy site. Similar figures are applicable for the clayey site as well. Consequently, the V_s profile with depth and the $G/G_{\max}$ versus γ curves for each layer also vary from sample to sample, as shown in Figure 4. The typical coefficient of variation values found for V_s and $G/G_{\max}$ are 0.12 and 0.32, respectively.

The spatial correlation among layers was characterized by a first-order auto-regressive model, with lag-one correlation coefficient equal to 0.58 (Toro, 1993). Since several borings at each site revealed similar lithologies, the thickness of each layer was not considered random. Within each layer in every simulation, a perfect positive correlation was assumed for Φ_0, G_0, and $\gamma_{64\%}$, and all three are considered to be perfectly negatively correlated with both ξ_s and ξ_c. K_0 and Φ_0 are assumed to be independent of all other RVs (F. Pelli, personal comm., 1998).

Amplification Study Results

Base Soil Column Case

For both sites, all the 78 records in the database were driven through the base-case soil column. For each analysis the $AF(f)$ is computed by dividing the response-spectrum ordinates of the ground motion at the surface by the corre-

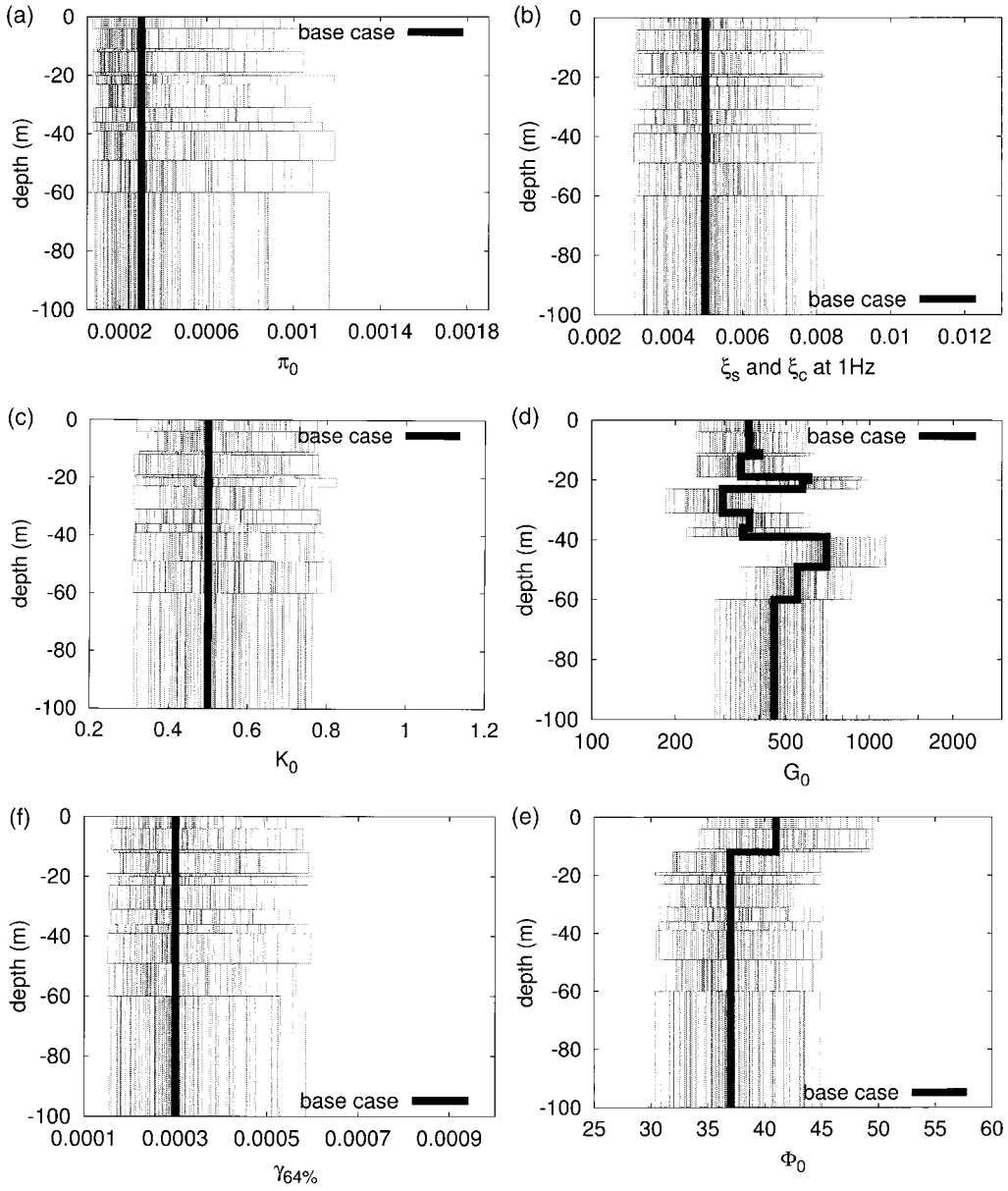

Figure 3. One hundred samples of randomized soil properties for the sandy site.

sponding response-spectrum ordinates of the accelerogram applied at the column base. For both sites the values of $S_a^r(f)$ and $S_a^s(f)$ for frequencies of 0.33 Hz, 1.0 Hz, 5.0 Hz, and 100 Hz (i.e., PGA) are reported in Table A2 in the Appendix. The 78 amplification functions are displayed in Figure 5 along with the mean, the median, and the mean plus and minus one standard deviation curve. In both cases, the two wide peaks at about 0.8–0.9 Hz and 2 Hz identify the first two soil resonant frequencies. On average, at $f_{sc} \approx 0.8$ to 0.9 Hz the sandy and clayey sites amplify, respectively, more than 3 and 4 times the spectral acceleration at the bedrock, $S_a^r(f_{sc})$. PGA_r is amplified, on average, by 40% and 100%, respectively.

In both cases, $AF(f)$ displays a large variability, particularly in the high-frequency range (more precisely, $\sigma_{\ln AF(f)}$ ranges from 0.25 at $f = 0.4$ Hz to 0.7 at $f = 15$ Hz as shown by the solid lines in Fig. 11a,b, which will be discussed later). Some of the records induce a highly nonlinear behavior in both soil deposits, with associated large deformations. The transfer functions generated by some of these severe accelerograms have values of 2 or less at frequencies about 1 Hz, values that decrease to below 1 at higher frequencies, and they do not exhibit the two distinct peaks previously mentioned. In some of these cases the top layers of the sandy site liquefy. However, liquefaction occurs at amplitude levels that are not constant but vary from record to record. This variability in the liquefaction threshold prevents abrupt changes in the median $AF(f)$ at specific intensity values of the input ground motion. On the other hand, some of the records generate $AF(f)$ curves well above 1 for the entire

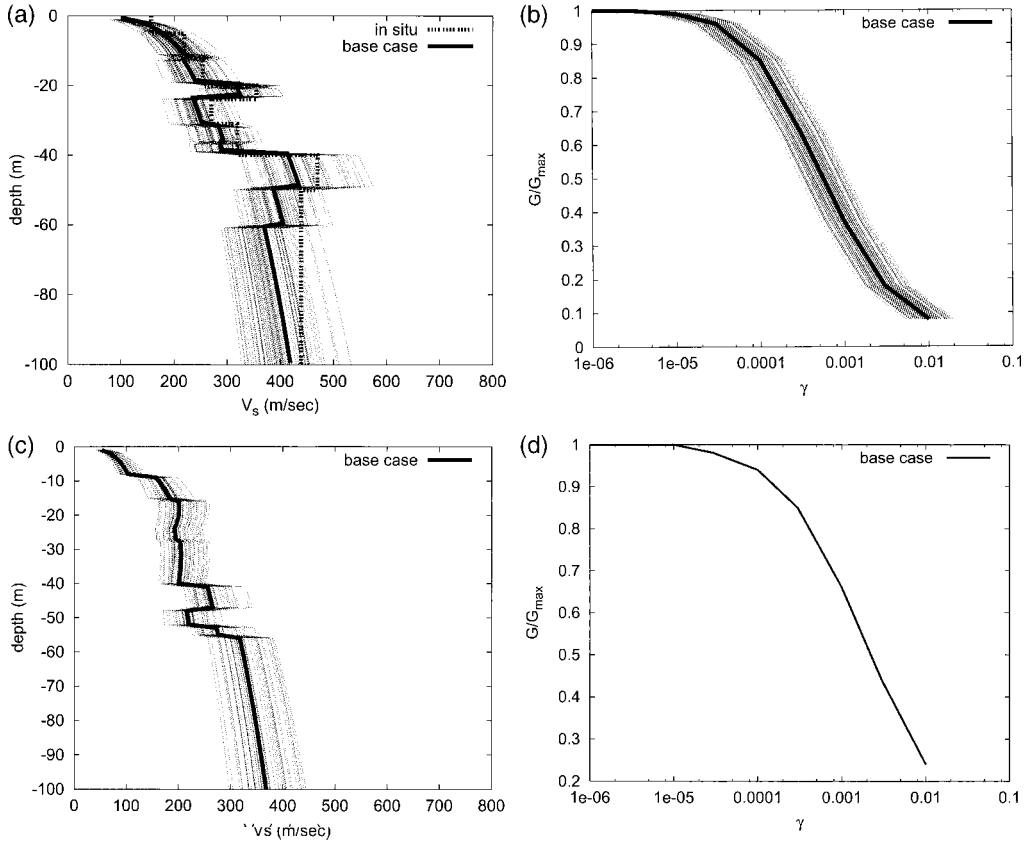

Figure 4. Panels a and b show the variability in V_s versus depth and in the G/G_{max} versus the γ curve in one of the soil layers (50 samples) for the sandy site. The V_s profile derived by *in situ* tests is also shown (panel a) for comparison. The same quantities are shown in panels c and d for one layer of the clayey site. The variability in the G/G_{max} curve, omitted in panel d, is similar to that displayed in panel b. The V_s profile recorded *in situ* for this latter case is not shown for confidentiality reasons.

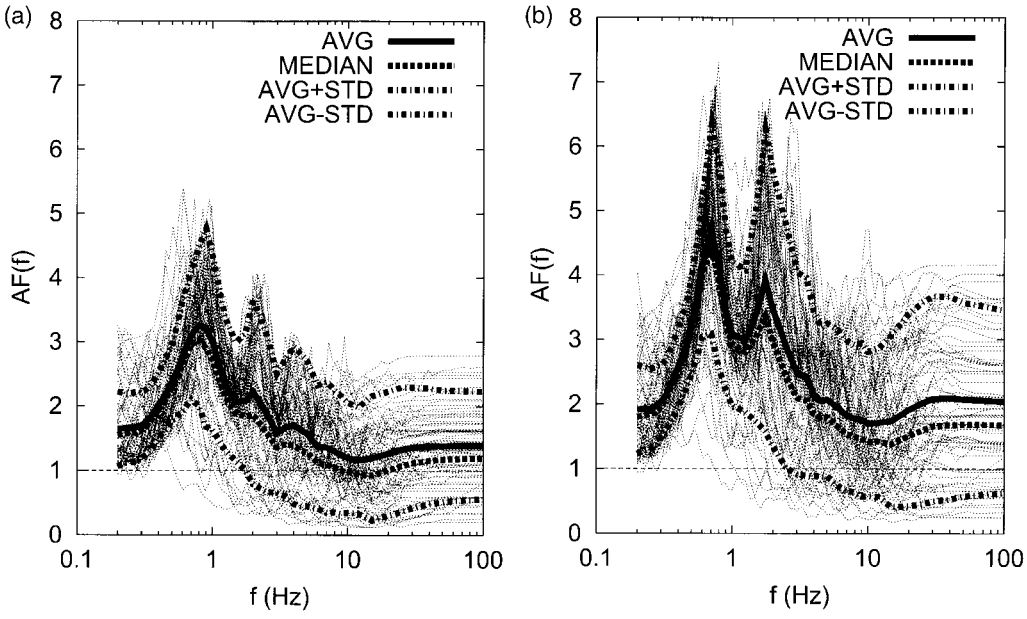

Figure 5. Amplification functions for the sandy site (panel a) and for the clayey site (panel b) (base case).

frequency range. As expected, this discrepancy is mostly due to the large differences in intensity of the input ground motions, as will become clear later.

The $AF(f)$, sorted by PGA_r and $S_a^r(f_{sc})$ values, are helpful in visually investigating the $AF(f)$ dependence on these two intensity measures of the input records. The amplification functions for the sandy site are presented in Figures 6 and 7, whereas those for the clayey site are displayed in Figures 8 and 9. The variability of $AF(f)$ reduces significantly in comparison to Figure 5. It is apparent that when the input intensity increases, the $AF(f)$ tends to diminish in amplitude and to flatten out. A systematic shift of the first (linear) resonant peak at f_{sc} ($\approx$0.9 Hz) toward lower frequencies when the intensity rises is also evident. As expected, PGA_r is a better discriminator between high and low $AF(f)$ at high f values, whereas $S_a^r(f_{sc})$ is more effective in the frequency range at about f_{sc} (as confirmed by Fig. 11c, d, to come). At frequencies lower than f_{sc} the dependence of $AF(f)$ on either one of the two intensity measures is not very pronounced, although a mild negative correlation with $S_a^r(f_{sc})$ (i.e., high values of $AF(f)$ tend to be generated by records with low $S_a^r(f_{sc})$ values) can be detected (Fig. 7f).

The effectiveness of a third, frequency-dependent rock ground-motion intensity, $S_a^r(f)$, in estimating $AF(f)$ (i.e., locally at the same frequency, f) can be appreciated by inspecting Figure 10, which displays the (log) quadratic-regression models fitted through the $AF(f)$ data from selected f values. The negative correlation between $AF(f)$ and $S_a^r(f)$ is evident for frequencies above f_{sc} and becomes stronger at higher frequencies. The linear and quadratic terms of the regression model are not statistically significant at f values below 0.75 Hz, as Figure 10a,b suggests.

The predictive power of several combinations of the five intensity variables mentioned earlier was formally studied via regression analysis. The goodness of such fits can be compared through standard deviation of the residual and coefficient of multiple determination (e.g., Neter *et al.*, 1990). Figure 11a,b show for both sites the residual standard deviation, $\sigma_{\ln AF(f)}$, of six of the most informative fitting equations among those investigated. (For simplicity, we have dropped from the notation $\sigma_{\ln AF(f)}$ the conditioning on the independent variables considered in each regression model, e.g., $\sigma_{\ln AF(f)|M,R}$.) For comparison, we included the unconditional $\sigma_{\ln AF(f)}$ curve, which describes the total variation in $AF(f)$ from Figure 5 where no regression is done. Note that the regressions in Figure 11 were observed to be homoscedastic. Fig. 11c,d displays the coefficient of multiple determination, R^2(adj), adjusted for its associated degrees of freedom. The value of R^2(adj) measures the proportionate reduction of total variation of $AF(f)$ that is gained from the use of the predictor variables (i.e., M, R, PGA_r, $S_a^r(f)$, and $S_a^r(f_{sc})$ here). Thus, the larger is R^2(adj); the more is the total variability of $AF(f)$ reduced by introducing the independent variables. Hence, R^2(adj) is a measure of the effectiveness of the model in predicting the dependent variable, here $AF(f)$.

We investigated, but did not include in Figure 11 for clarity of representation, the models with $S_a^r(f)$ and M, or PGA_r and M. The $\sigma_{\ln AF(f)}$ and R^2(adj) curves for such models were found to be indistinguishable in the frequency range above f_{sc} from those of the corresponding models without M (i.e., open triangles and diamonds in Fig. 11). In the frequency range below f_{sc} the omitted curves are coincident with those generated by the M and R model (marked with crosses in Fig. 11). This subject is discussed further as follows.

From inspecting Figure 11 it appears that, despite the significant differences in the soil conditions, the results for both sites are surprisingly consistent. It is also evident that the explanatory power of the independent variables is much less in the frequency range below f_{sc} (and especially below 0.5 Hz) than it is above, where the explained variation is as high as approximately 90% (Fig. 11c,d). For clarity, it is useful to comment separately on the prediction of $AF(f)$ in the two frequency ranges below and above f_{sc} (i.e., about 0.8 to 0.9 Hz).

In the frequency range below f_{sc}, $AF(f)$ is virtually independent of any single intensity of the ground motion, such as $S_a^r(f)$, $S_a^r(f_{sc})$ and PGA_r. This can be appreciated from Figure 10a,b and also from Figure 11 by comparing the unconditional $\sigma_{\ln AF(f)}$ curve for $f < f_{sc}$ with all the others. Adding M to the models in $S_a^r(f)$, $S_a^r(f_{sc})$, or PGA_r slightly improves the prediction but produces R^2(adj) values (not shown in Fig. 11) equal to those of the M and R model (i.e., only 25% or lower) when the intensity measure is not included in the model. The results in Figure 12, obtained for the clayey site (similar results apply for the sandy site), reinforce the evidence that given $S_a^r(f)$, the magnitude M, which carries implicitly information on spectral shape and ground-motion duration, can be a moderately useful predictor variable exclusively in this low-frequency range (for practical purposes only the difference between predictive equations for $M5$ and $M8$ is noteworthy).

In the frequency range below f_{sc} (and especially below 0.5 Hz), more effective than any model with M in estimating $AF(f)$ is the one that includes both $S_a^r(f)$ and $S_a^r(f_{sc})$. This latter model at oscillator frequencies of 0.33 and 0.25 Hz explains up to 50% to 60% of the variability in $AF(f)$, a substantial increase from only the 10% to 20% explained by the best of all the other predictive equations. In this frequency range $AF(f)$ is in fact negatively correlated with $S_a^r(f)$ and positively correlated with $S_a^r(f_{sc})$. A higher $S_a^r(f)$ value tends to reduce $AF(f)$ because of nonlinearities in the soil response, whereas a higher $S_a^r(f_{sc})$ tends to increase $AF(f)$ because of the resonant-frequency shift toward lower values. We suspect that M explains part of the variability of $AF(f)$ in this frequency range because it implies something about spectral shape, and therefore it carries information about the expected values of $S_a^r(f)$ and $S_a^r(f_{sc})$ for any given distance. Finally, note that despite the difficulty in obtaining important predictive models in the range below f_{sc} (the unconditional $\sigma_{\ln AF(f)}$ values are already comparatively low

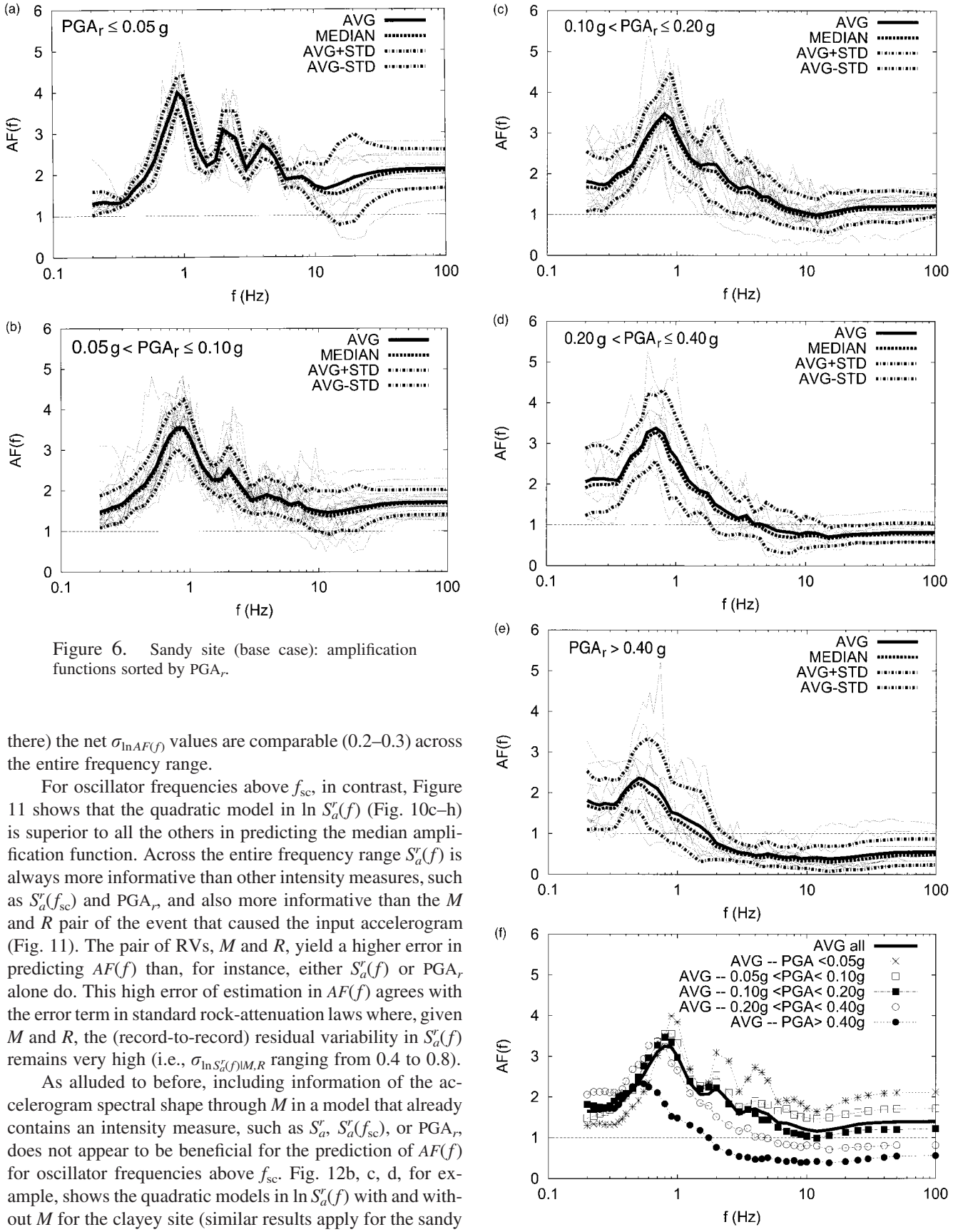

Figure 6. Sandy site (base case): amplification functions sorted by PGA$_r$.

there) the net $\sigma_{\ln AF(f)}$ values are comparable (0.2–0.3) across the entire frequency range.

For oscillator frequencies above f_{sc}, in contrast, Figure 11 shows that the quadratic model in $\ln S_a^r(f)$ (Fig. 10c–h) is superior to all the others in predicting the median amplification function. Across the entire frequency range $S_a^r(f)$ is always more informative than other intensity measures, such as $S_a^r(f_{sc})$ and PGA$_r$, and also more informative than the M and R pair of the event that caused the input accelerogram (Fig. 11). The pair of RVs, M and R, yield a higher error in predicting $AF(f)$ than, for instance, either $S_a^r(f)$ or PGA$_r$ alone do. This high error of estimation in $AF(f)$ agrees with the error term in standard rock-attenuation laws where, given M and R, the (record-to-record) residual variability in $S_a^r(f)$ remains very high (i.e., $\sigma_{\ln S_a^r(f)|M,R}$ ranging from 0.4 to 0.8).

As alluded to before, including information of the accelerogram spectral shape through M in a model that already contains an intensity measure, such as S_a^r, $S_a^r(f_{sc})$, or PGA$_r$, does not appear to be beneficial for the prediction of $AF(f)$ for oscillator frequencies above f_{sc}. Fig. 12b, c, d, for example, shows the quadratic models in $\ln S_a^r(f)$ with and without M for the clayey site (similar results apply for the sandy site). For frequencies above f_{sc} including or neglecting M yields the same predictive equations for $AF(f)$. The explan-

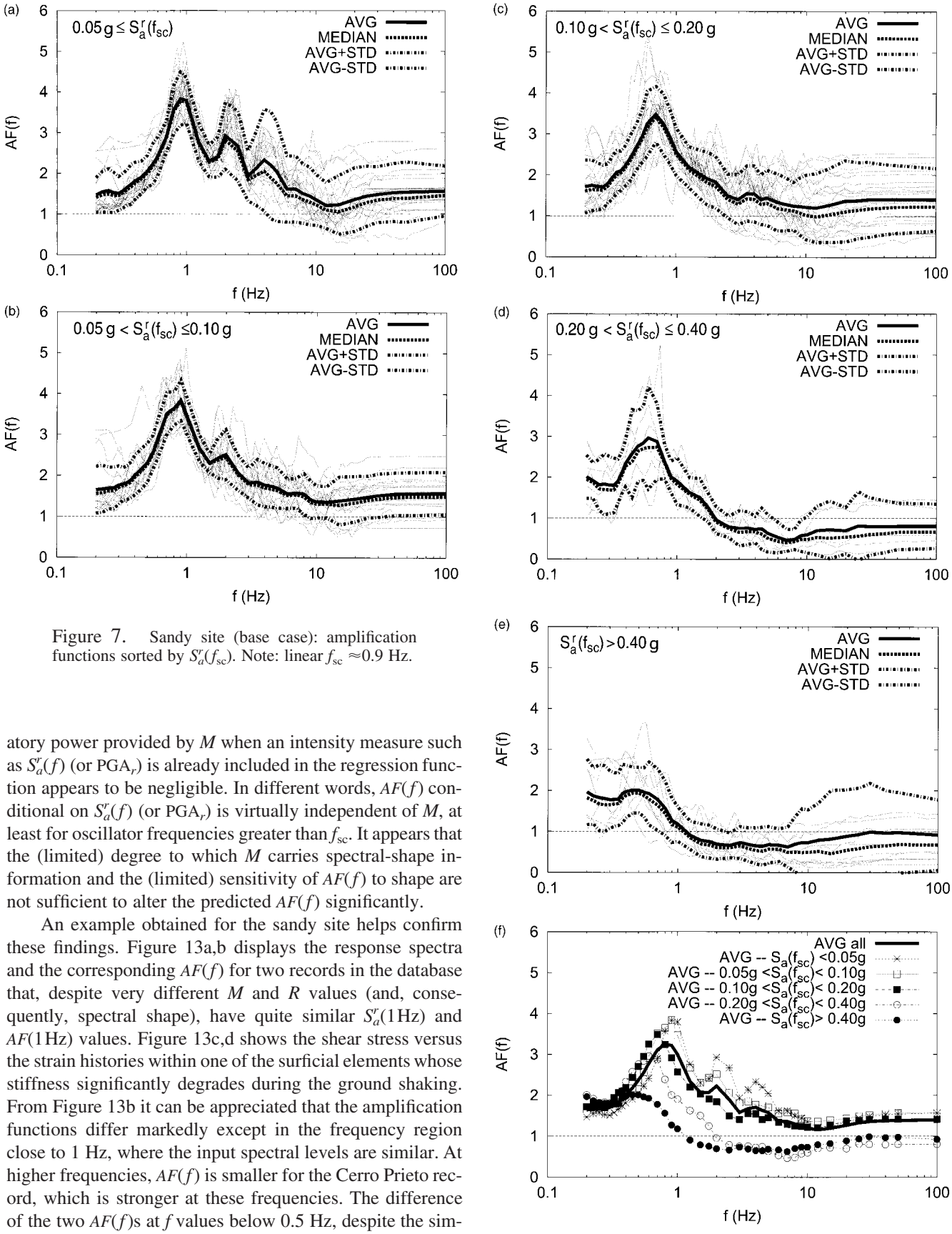

Figure 7. Sandy site (base case): amplification functions sorted by $S_a^r(f_{sc})$. Note: linear $f_{sc} \approx 0.9$ Hz.

atory power provided by M when an intensity measure such as $S_a^r(f)$ (or PGA_r) is already included in the regression function appears to be negligible. In different words, $AF(f)$ conditional on $S_a^r(f)$ (or PGA_r) is virtually independent of M, at least for oscillator frequencies greater than f_{sc}. It appears that the (limited) degree to which M carries spectral-shape information and the (limited) sensitivity of $AF(f)$ to shape are not sufficient to alter the predicted $AF(f)$ significantly.

An example obtained for the sandy site helps confirm these findings. Figure 13a,b displays the response spectra and the corresponding $AF(f)$ for two records in the database that, despite very different M and R values (and, consequently, spectral shape), have quite similar $S_a^r(1\text{Hz})$ and $AF(1\text{Hz})$ values. Figure 13c,d shows the shear stress versus the strain histories within one of the surficial elements whose stiffness significantly degrades during the ground shaking. From Figure 13b it can be appreciated that the amplification functions differ markedly except in the frequency region close to 1 Hz, where the input spectral levels are similar. At higher frequencies, $AF(f)$ is smaller for the Cerro Prieto record, which is stronger at these frequencies. The difference of the two $AF(f)$s at f values below 0.5 Hz, despite the similarity in the input, is an example of the limited dependence of $AF(f)$ on $S_a^r(f)$ in that frequency range.

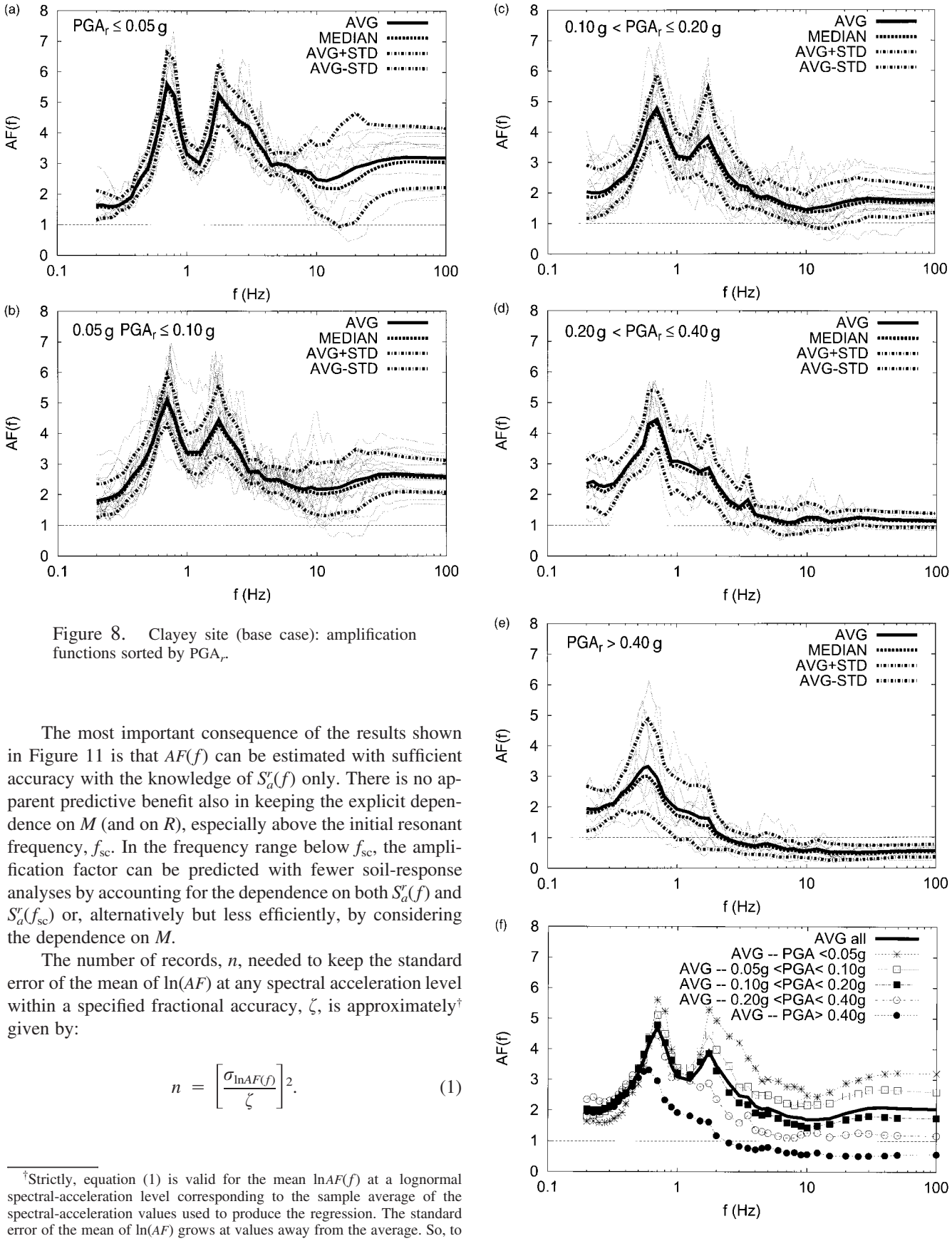

Figure 8. Clayey site (base case): amplification functions sorted by PGA$_r$.

The most important consequence of the results shown in Figure 11 is that $AF(f)$ can be estimated with sufficient accuracy with the knowledge of $S_a^r(f)$ only. There is no apparent predictive benefit also in keeping the explicit dependence on M (and on R), especially above the initial resonant frequency, f_{sc}. In the frequency range below f_{sc}, the amplification factor can be predicted with fewer soil-response analyses by accounting for the dependence on both $S_a^r(f)$ and $S_a^r(f_{sc})$ or, alternatively but less efficiently, by considering the dependence on M.

The number of records, n, needed to keep the standard error of the mean of ln(AF) at any spectral acceleration level within a specified fractional accuracy, ζ, is approximately† given by:

$$n = \left[\frac{\sigma_{\ln AF(f)}}{\zeta}\right]^2. \quad (1)$$

†Strictly, equation (1) is valid for the mean ln$AF(f)$ at a lognormal spectral-acceleration level corresponding to the sample average of the spectral-acceleration values used to produce the regression. The standard error of the mean of ln(AF) grows at values away from the average. So, to maximize accuracy, the record intensities should be chosen in the appropriate ln $S_a(f)$ neighborhood.

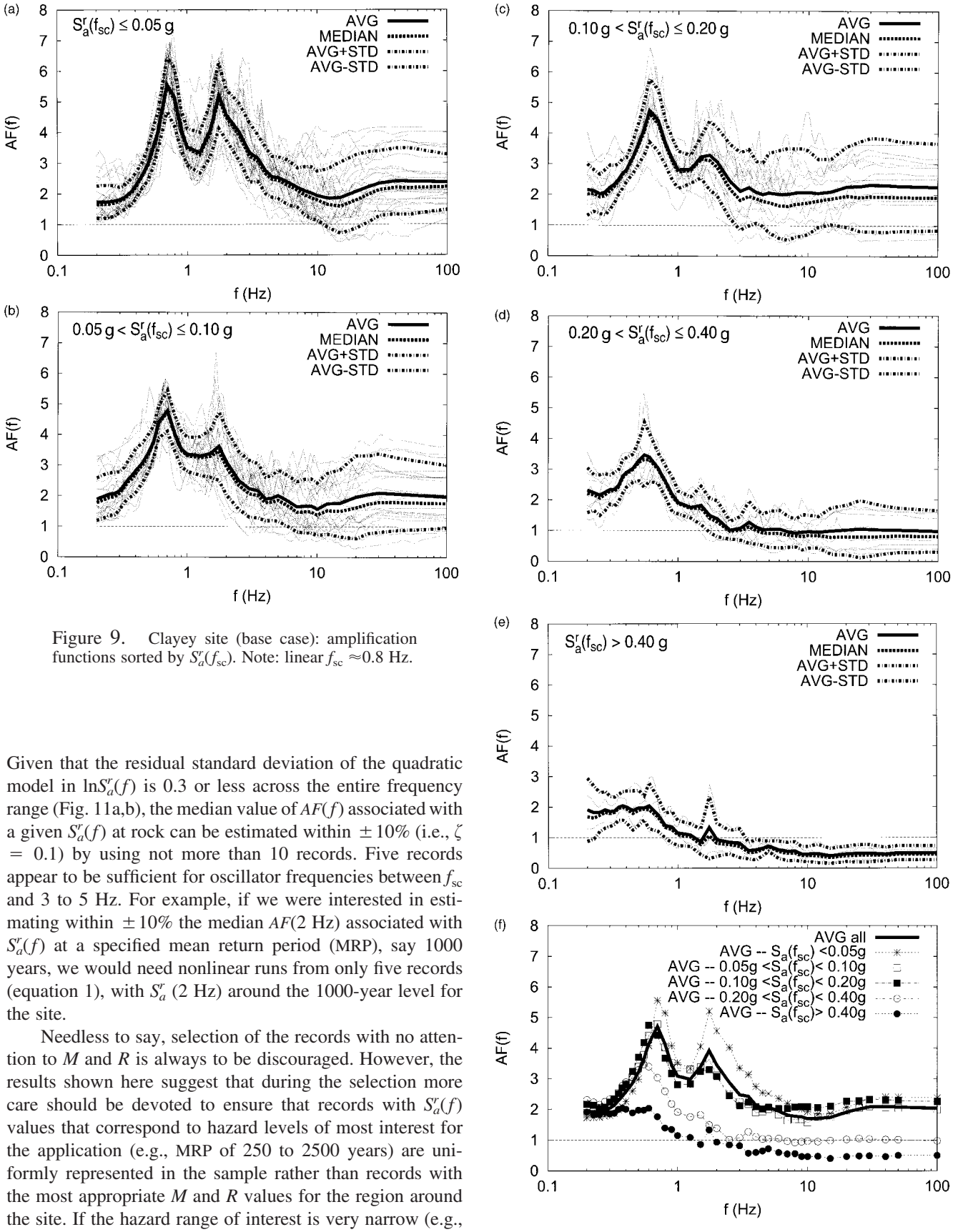

Figure 9. Clayey site (base case): amplification functions sorted by $S_a^r(f_{sc})$. Note: linear $f_{sc} \approx 0.8$ Hz.

Given that the residual standard deviation of the quadratic model in $\ln S_a^r(f)$ is 0.3 or less across the entire frequency range (Fig. 11a,b), the median value of $AF(f)$ associated with a given $S_a^r(f)$ at rock can be estimated within $\pm 10\%$ (i.e., $\zeta = 0.1$) by using not more than 10 records. Five records appear to be sufficient for oscillator frequencies between f_{sc} and 3 to 5 Hz. For example, if we were interested in estimating within $\pm 10\%$ the median $AF(2\text{ Hz})$ associated with $S_a^r(f)$ at a specified mean return period (MRP), say 1000 years, we would need nonlinear runs from only five records (equation 1), with S_a^r (2 Hz) around the 1000-year level for the site.

Needless to say, selection of the records with no attention to M and R is always to be discouraged. However, the results shown here suggest that during the selection more care should be devoted to ensure that records with $S_a^r(f)$ values that correspond to hazard levels of most interest for the application (e.g., MRP of 250 to 2500 years) are uniformly represented in the sample rather than records with the most appropriate M and R values for the region around the site. If the hazard range of interest is very narrow (e.g., MRP of 1000 years only), it is beneficial for a more accurate estimate of the slope of the $AF(f)$ model to select records

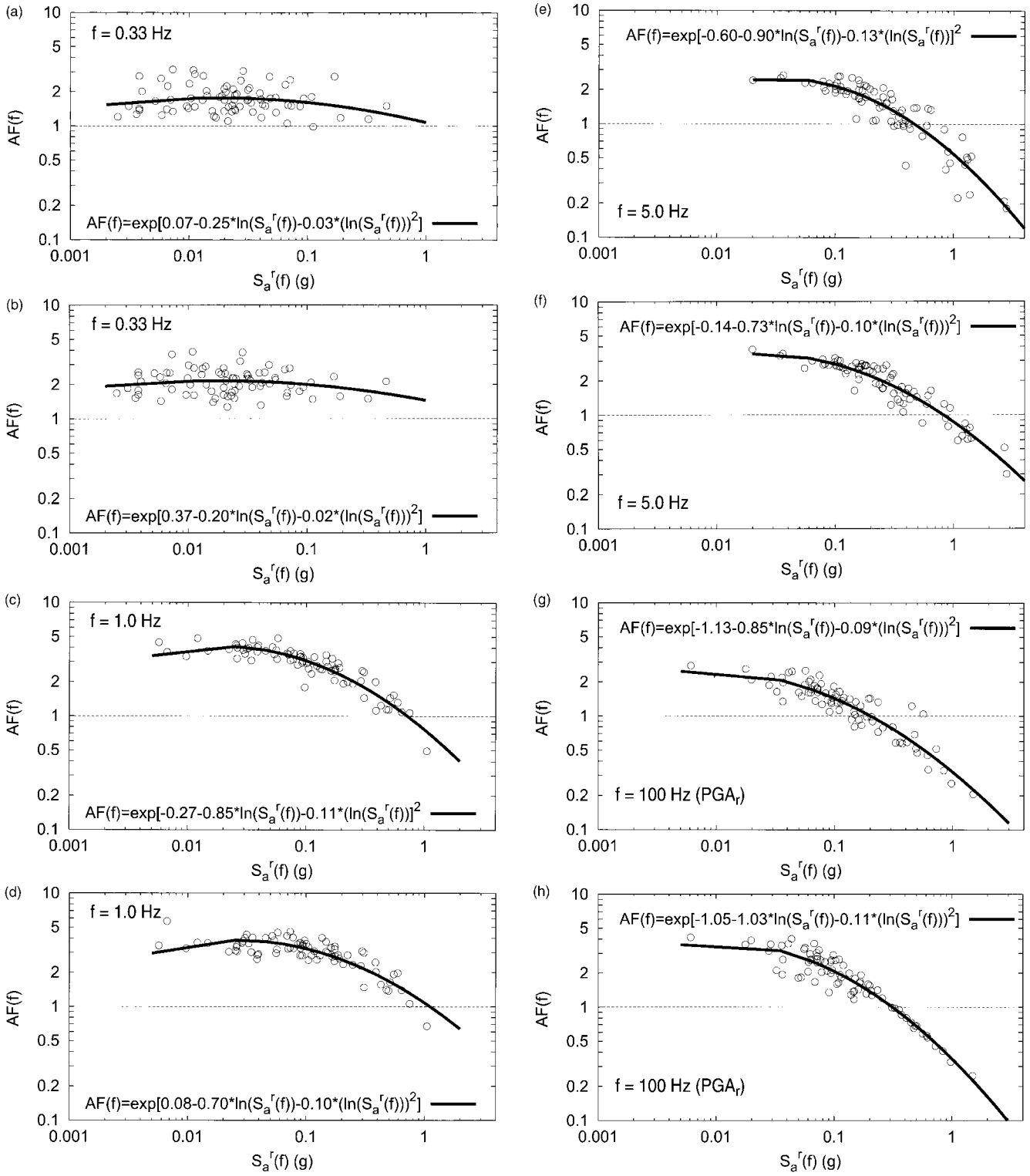

Figure 10. Regression for both sites of $AF(f)$ on $S_a^r(f)$ at different f values. (Sandy site in panels a, c, e, and g. Clayey site in panels b, d, f, and h.)

that have $S_a^r(f)$ in the neighborhood of the target hazard level. Attention to the magnitude of the records employed should be used when the application at hand requires an accurate estimate of $AF(f)$ at very short oscillator frequency. These results should simplify record selection during site-specific studies of the amplification function, because the same suite of records can be used to study $AF(f)$ at all frequencies.

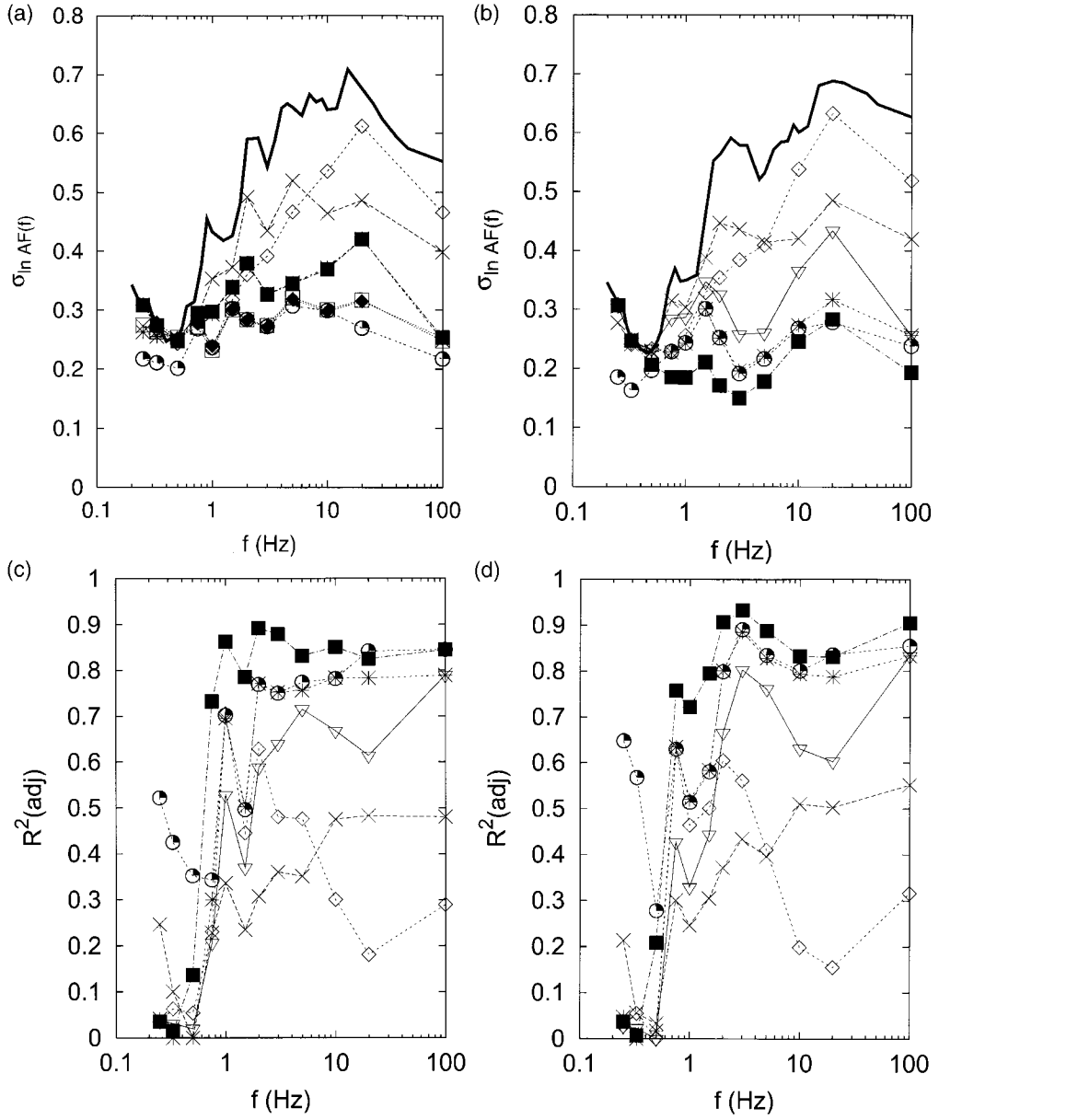

Figure 11. Regression of $AF(f)$ on M, R, PGA_r, $S_a^r(f)$, and $S_a^r(f_{sc})$ for the sandy site in panels a and c, and for the clayey site in panels b and d. Legend: $\sigma_{\ln AF(f)}$ = residual standard deviation; R^2(adj) = coefficient of multiple determination.

Randomized Soil Column Case

To study the effect of the uncertainty of the soil properties on the amplification function and the conclusions presented, each accelerogram in the database was driven through a different sample of each of the two soil columns. The 78 $AF(f)$ curves are shown in Figure 14 (to be compared with Fig. 5). The average $AF(f)$ lines for this randomized set, owing to the slight shifts in resonant frequencies for different soil-column samples, appear to be smoother than those for the base case (Fig. 15a). Only in a few extreme

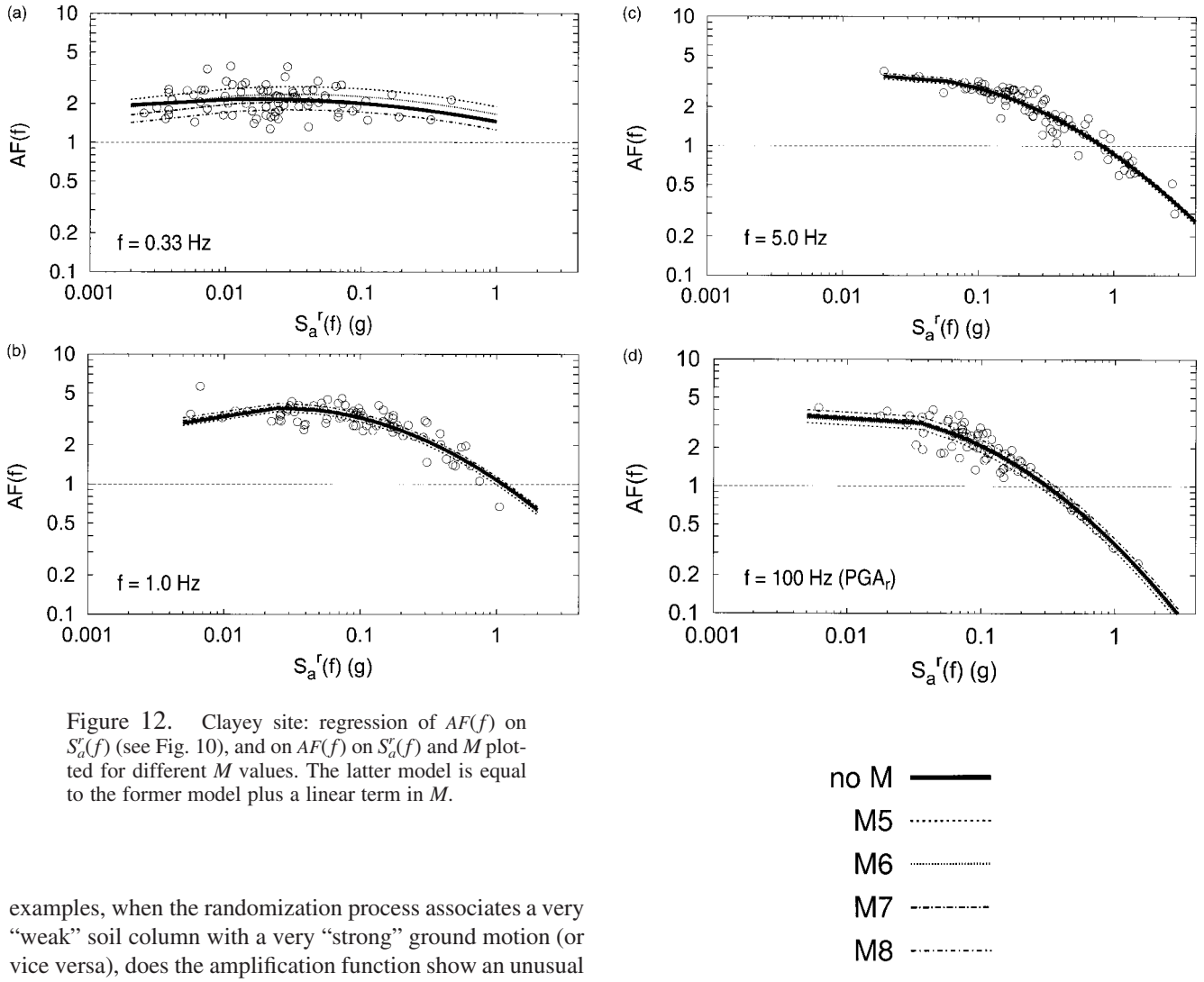

Figure 12. Clayey site: regression of $AF(f)$ on $S_a^r(f)$ (see Fig. 10), and on $AF(f)$ on $S_a^r(f)$ and M plotted for different M values. The latter model is equal to the former model plus a linear term in M.

examples, when the randomization process associates a very "weak" soil column with a very "strong" ground motion (or vice versa), does the amplification function show an unusual pattern in comparison to the corresponding one for the base case.

From visual inspection of Figures 5 and 14, the extra variability introduced by the randomization process appears to be of secondary importance in comparison to the record-to-record variability of the base case. This is confirmed by Figure 15b, which shows that the unconditional $\sigma_{\ln AF(f)}$ curves are indeed similar for both the base case and the randomized case sets. The extra source of variability in the soil input parameters results in an increase in the $\sigma_{\ln AF(f)}$ curves, more noticeable in the low-frequency range. From Figure 15b (and from Fig. 16 to come) the variability in $AF(f)$ owing to the uncertainty in the soil parameters appears to be comparable in magnitude to the record-to-record variability in $AF(f)$ only at frequencies lower than f_{sc}. For f values above f_{sc}, the unconditional $\sigma_{\ln AF(f)}$ curve derived from the analyses with uncertain soil parameters is less than 20% larger than the curve for the base case.

The variability in $AF(f)$ owing solely to the uncertain soil characteristics, $[\sigma_{\ln AF(f)}]_{soil}$, can be separated out from the record-induced variability by running each accelerogram through multiple realizations of the soil column. For this purpose we obtained for the sandy site 78 samples of $[\sigma_{\ln AF(f)}]_{soil}$ at each frequency f of interest by performing 10 analyses for each of the 78 records in the database, for a total of 780 analyses. The average $[\sigma_{\ln AF(f)}]_{soil}$ versus f curve, and the average plus and minus 1 standard deviation curves plotted versus frequency, are displayed in Figure 16. In this case the average $[\sigma_{\ln AF(f)}]_{soil}$ is always less than 0.3 for any f. The average $AF(f)$ and the unconditional $\sigma_{\ln AF(f)}$ curves displayed in Figure 15 for the randomized case are statistically indistinguishable from those (not shown in the figure) produced by this set of 780 analyses. This implies that there is no need to perform multiple runs of different soil-column samples with the same record in order to capture the variability in $AF(f)$ owing to soil-parameter uncertainty. Driving each accelerogram through a different soil-column characterization is sufficient.

Finally, including the variability in $AF(f)$ owing to the uncertainty in the soil parameters does not modify the conclusions drawn from the results of multiple-regression analyses shown in Figure 11 for the base case. Only the residual standard deviation in each model increases slightly when

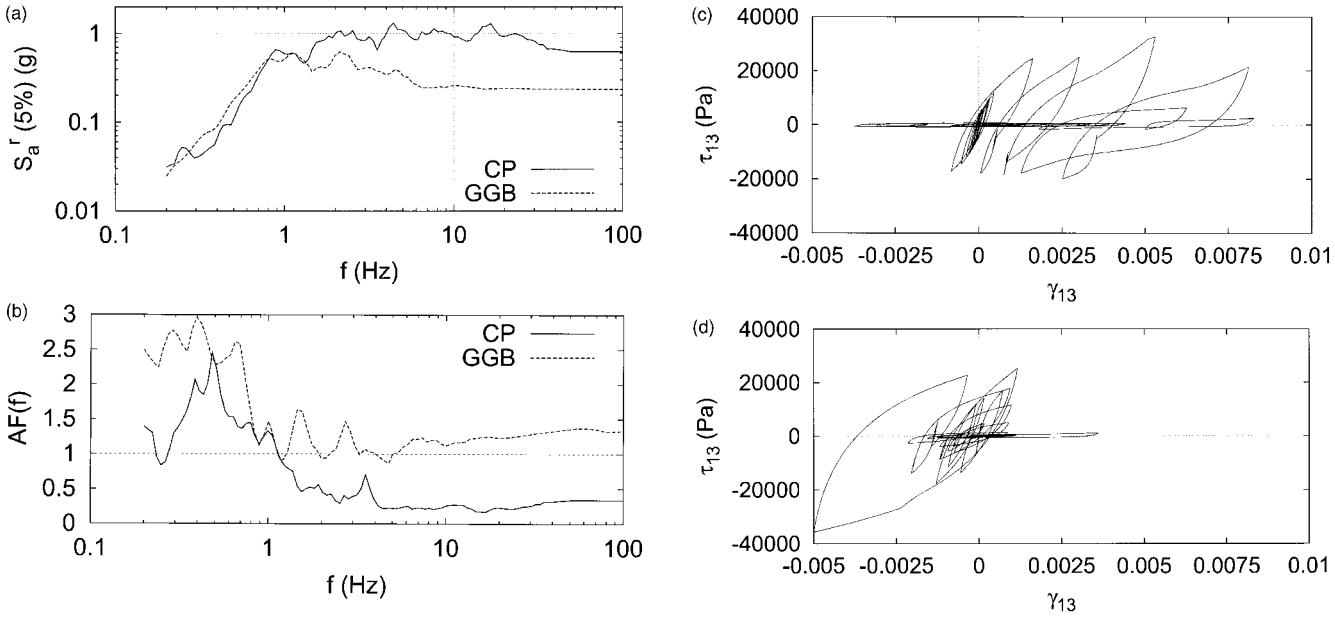

Figure 13. Results for the 1980 M 6.1 Victoria earthquake, Cerro Prieto (CP) record, and the 1989 M 6.9 Loma Prieta earthquake, Golden Gate Bridge (GGB) record. Panels c and d show the shear stress versus the strain history in the sandy soil deposit at 6.5 below the seabed.

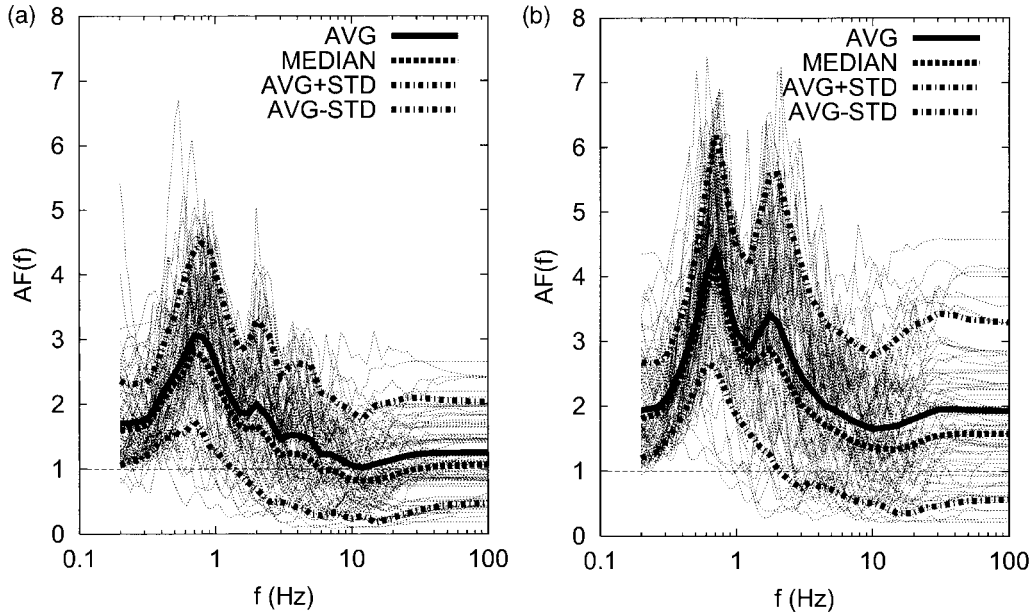

Figure 14. Amplification functions for both soil deposits (randomized soil properties). (Sandy site in panel a, and clayey site in panel b.)

compared with those for the base-case set. For example, for the randomized case the residual standard deviation of the (log) quadratic model in $\ln S_a^r(f)$ maintains the same pattern as in Figure 11a,b, but on average (across frequency) the values of about 0.15 to 0.30 found for the base case are increased here by 10% to 15%. Hence, even when the soil uncertainty is included in the modeling, the median value of $AF(f)$ associated with a given $S_a^r(f)$ at rock can still be estimated within $\pm 10\%$ by using not more than 8 to 13 records.

Further, including this extra source of uncertainty changed none of the conclusions regarding the limited benefit in adding M as an independent variable, given that $S_a^r(f)$ was already included in the model for $AF(f)$ prediction.

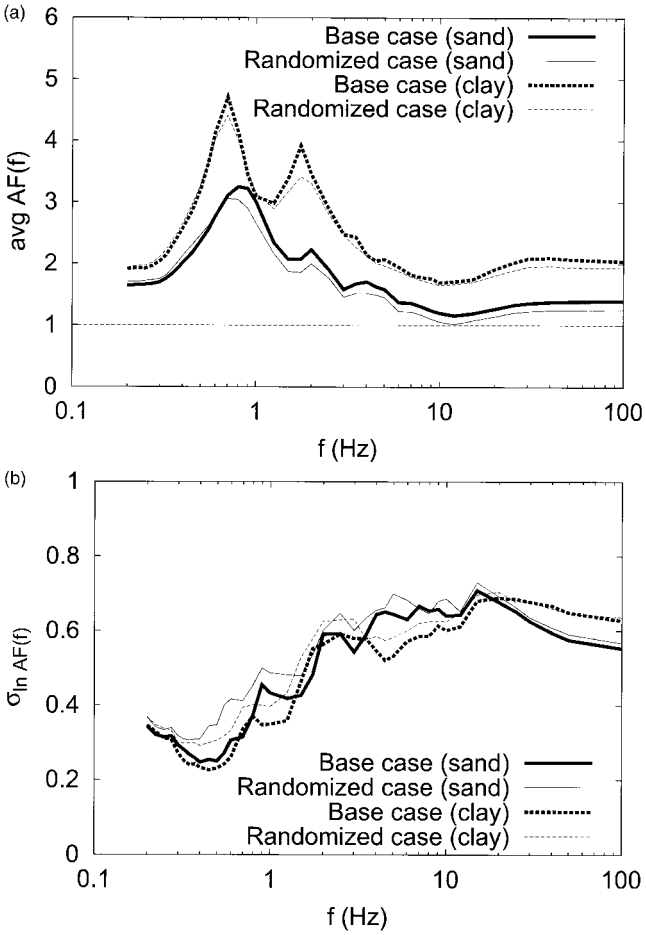

Figure 15. Comparison of average $AF(f)$ and unconditional $\sigma_{\ln AF(f)}$ curves obtained from the base case and the randomized case sets.

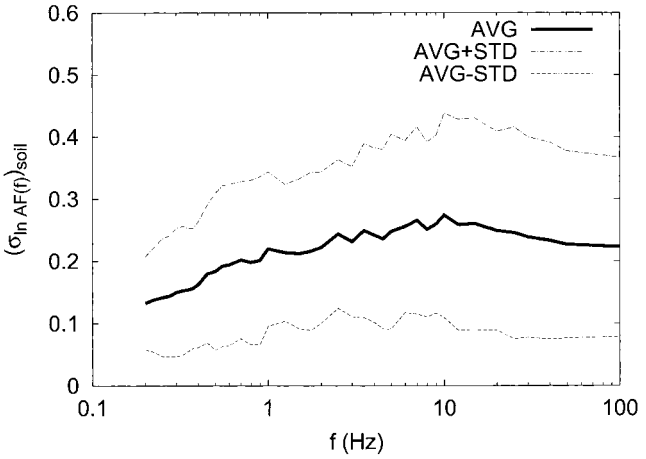

Figure 16. Variability in $AF(f)$ owing to the uncertainty in the soil properties at the sandy site. The standard deviation of $(\sigma_{\ln AF(f)})_{\text{soil}}$ is due to record-to-record variability.

Range of Applicability of the Statistical Results

The statistical results found in this article were confirmed by additional applications (e.g., Pelli *et al.*, 2004) involving onshore soil columns that are prevalently stiffer and/or stronger and less nonlinear than these two offshore soil-column cases. In particular, the limited conditional dependency of $AF(f)$ on M, and the secondary importance of the variability in $AF(f)$ induced by the uncertainty in the soil parameters in comparison to the contribution of the record-to-record variability, were consistently observed. These two primary statistical properties of $AF(f)$ were also found in two alternative modifications of the clayey-soil-column example, where the soil was forced to respond linearly to the ground shaking. In the first alternative all the soil parameters were considered deterministic and kept constant throughout all the response analyses, whereas in the second alternative the same set of properties discussed in the subsection on soil modeling were allowed to vary according to predefined distributions and correlation structure. The residual standard deviation of the (log) quadratic model in $\ln S_a^r(f)$ across the entire frequency range was less than 20% larger in the latter (random) case than in the former (deterministic) case.

Conclusions

In this study we have investigated from a statistical perspective the effect of soil layers with uncertain properties on the amplification of surface ground motion with respect to incident bedrock motion. The nonlinear response of the soil was considered here in terms of the spectral-acceleration, frequency-dependent amplification function, $AF(f)$, for a wide range of oscillator frequency, f. The uncertainty of the soil properties and the imperfect correlation of the parameter values in different layers were considered via a Monte Carlo simulation procedure. The site amplification of two nonlinear offshore soil deposits, one sandy and one clayey, was considered here.

The response computations were performed by means of a finite-element computer program capable of modeling the soil nonlinearity during ground shaking, including water pore-pressure buildup and dissipation. Each soil column was subjected to a suite of real rock recordings applied to its base, and the $AF(f)$ was computed for each run.

As expected, multiple-regression analyses performed on the $AF(f)$ datasets at f values ranging from 0.25 to 100 Hz (i.e., PGA) consistently revealed that $AF(f)$ for both sites is strongly dependent on the intensity of the input ground motion at the same oscillator frequency, $S_a^r(f)$. This is especially true above a threshold value around the initial resonant frequency, f_{sc}, of the soil columns (here 0.8 to 0.9 Hz). Other intensity measures of the input record, such as the peak ground acceleration, PGA_r, are found to be less useful predictors than $S_a^r(f)$. If the $S_a^r(f)$ value of the bedrock accelerogram is known, the information on the magnitude, M, of the earthquake that caused it does not significantly improve

the prediction of $AF(f)$ for frequencies above f_{sc}. The amplification function at the frequency $f < f_{sc}$ is more efficiently estimated by using the knowledge of both $S_a^r(f)$ and $S_a^r(f_{sc})$, the spectral acceleration at the initial fundamental frequency of the soil, and, to a lesser degree, of both $S_a^r(f)$ and M. M, in fact, has a bearing on the spectral shape and therefore on the average value of $S_a^r(f_{sc})$, given $S_a^r(f)$. Note that for stiffer sites the fundamental frequency $f < f_{sc}$ can be considerably higher than the values of 0.8–0.9 Hz shown in these two examples.

The lack of strong M dependence of $AF(f)$ given $S_a^r(f)$ and the small record-to-record variability of $AF(f)$ conditional on $S_a^r(f)$ in comparison to the inherent record-to-record variability of $S_a^r(f)$ have some important practical consequences.

The median $AF(f)$ for the entire frequency range can be estimated with sufficient accuracy by driving 10 or fewer ground-motion recordings through a different characterization of the soil column. It is emphasized, however, that the extra variability of $AF(f)$ owing to the uncertainty in the soil (at least for the amount of variability in the soil properties addressed here) is of secondary importance in comparison to the record-to-record variability of $AF(f)$ observed when using the best estimate of each soil parameter. Regression analysis can be used to derive the best fitting equation in (log) $S_a^r(f)$ for the prediction of the median $AF(f)$. A quadratic form was found effective.

These results imply further that (at least with respect to the soil-amplification problem) it is not critical to select with great precision the records representing the scenario events (i.e., M and R pairs) dominating the site hazard. In particular, it should not be necessary to be highly concerned about frequency dependence of the scenario events or, therefore, about using the same records to study $AF(f)$ at all frequency ranges for these two studies. In practice, this can greatly simplify the site-specific study of the amplification function.

To conclude, it is important to emphasize that this methodology is not restricted or specifically designed for offshore applications. Additional analyses (not included in this article) have shown that the two primary statistical properties of $AF(f)$ (i.e., the limited dependence of $AF(f)$ on M, given $S_a^r(f)$, and the limited contribution to the total variability in $AF(f)$ generated by the random soil properties) hold also for onshore unsaturated or partially saturated sites that are stronger and/or stiffer (and less nonlinear) than those shown here. These statistical properties are also valid for the extreme case of a linear soil column.

Our companion article in this issue (Bazzurro and Cornell, 2004) presents a procedure that integrates these findings in conventional probabilistic seismic hazard analysis (PSHA) to provide soil-specific hazard estimates at a given site.

Acknowledgments

The authors gratefully acknowledge the financial support of the U.S. Nuclear Regulatory Commission through Contract NRC-04-95-075 and of the National Science Foundation through Contract CMS 9423596. Deep appreciation is expressed to Dr. Fabrizio Pelli, who has provided us, in addition to the soil data and SUMDES models, with the necessary expertise in soil dynamics, and to Mauro Mangini and Edoardo Lanata for having run some additional analyses. This work has also benefited greatly from the many fruitful discussions with Dr. Norman Abrahamson and Dr. Walter Silva. They also placed at our disposal the PSHA software, the seismotectonic data, and the uniformly processed ground-motion database. We also thank Drs. William Joyner, David Boore, Robin McGuire, and Robert Pyke and two anonymous reviewers for their insightful comments.

References

Abrahamson, N. A. (1996). Empirical models of site response effects, in *Proc. of the 11th World Conf. on Earthquake Engineering*, Acapulco, Mexico, 23–28 June 1996, Paper No. 2042.

Abrahamson, N. A., and W. J. Silva (1997). Empirical response spectra attenuation relations for shallow crustal earthquakes, *Seism. Res. Lett.* **68,** 94–127.

Bazzurro, P., and C. A. Cornell (2004). Nonlinear soil-site effects in probabilistic seismic-hazard analysis, *Bull. Seism. Soc. Am.* **96,** 2110–2123.

Costantino, C. J., C. A. Miller, and E. Heymsfield (1993). Site specific seismic hazard calculations at deep soil sites, in *Proc. of the 4th U.S. Department of Energy Natural Phenomena Hazards Mitigation Conf.*, LLNL CONF-9310102, 199–205.

Electric Power Research Institute (1993). Guidelines for site specific ground motions, Rept. TR-102293, Vol. 1–5, Palo Alto, California.

Faccioli, E. (1976). A stochastic approach to soil amplification, *Bull. Seism. Soc. Am.* **66,** 1277–1291.

Hwang, H. H. M., and J.-R. Huo (1994). Generation of hazard-consistent ground motion, *J. Soil Dyn. and Earthquake Eng.* **13,** 377–386.

Kramer, S. L. (1996). *Geotechnical Earthquake Engineering*, Int. Series in Civil Engineering and Engineering Mechanics, Prentice Hall, New York.

Lee, R., W. J. Silva, and C. A. Cornell (1998). Alternatives in evaluating soil- and rock-site seismic hazard (abstract), *Seism. Res. Lett.* **69,** 81.

Li, X. S., C. K. Shen, and Z. L. Wang (1998). Fully coupled inelastic site response analysis for 1986 Lotung earthquake, *J. of Geotech. and Geoenviron. Eng.* **124,** 561–573.

Li, X. S., Z. L. Wang, and C. K. Shen (1992). SUMDES: a nonlinear procedure for response analysis of horizontally-layered sites subjected to multi-directional earthquake loading, Dept. of Civil Engineering, Univ. of California, Davis.

Neter, J., W. Wasserman, and M. H. Kutner (1990). *Applied Linear Statistical Models*, Third Ed., Irwin, Homewood, Illinois.

Ni, S.-D., R. V. Siddharthan, and J. G. Anderson (1997). Characteristics of nonlinear response of deep saturated soil deposits, *Bull. Seism. Soc. Am.* **87,** 342–355.

Pelli, F., P. Bazzurro, M. Mangini, and D. Spallarossa (2004). Probabilistic seismic hazard mapping with site amplification effects in *Proc. of the 11th International Conf. on Soil Dynamics and Earthquake Engineering*, Berkeley, California, 7–9 January 2004, Vol. 2, pp. 230–237.

Schnabel, P., H. B. Seed, and J. Lysmer (1972). Modification of seismograph records for effect of local soil conditions, *Bull. Seism. Soc. Am.* **62,** 1649–1664.

Silva, W. J. (1993). "Factors controlling strong ground motions and their associated uncertainties," in Seismic and Dynamic Analysis and Design Considerations for High Level Nuclear Waste Repositories, American Society of Civil Engineers, pp. 132–161.

Silva, W. (1997a). Description and validation of the stochastic ground motion model, prepared for Brookhaven National Laboratory, Associated Universities, Inc., Upton, New York.

Silva, W. (1997b). Earthquake ground motion database, Pacific Engineering and Analysis, El Cerrito, California.

Steidl, J. H., A. G. Tumarkin, and R. J. Archuleta (1996). What is a reference site?, *Bull. Seism. Soc. Am.* **86,** 1733–1748.

Toro, G. (1993). Probabilistic model of soil-profile variability, in *Guidelines for Determining Design Basis Ground Motions*, Schneider, J. F. (Editor), Electric Power Research Institute, EPRI TR-102293, Vol. 2, Appendix 6A.

Tsai, C.-C., P. (2000). Probabilistic seismic hazard analysis considering nonlinear site effects, *Bull. Seism. Soc. Am.* **90,** 1–7.

Whitman, R. V., and J. N. Protonotarios (1977). Inelastic response to site-modified ground motions, *J. of Geotech. Eng. Div.*, American Society of Civil Engineers **103,** 1037–1053.

Appendix

Table A1

Ground Motions Included in the Database

Earthquake							
No.	Name	Station Name	Date	Comp.	Mag.	Dist. (km)	$V s_{30}$ (m/sec)
1	Parkfield	Cholame #2	06-28-66	065	6.1	0.1	409
2	Parkfield	Temblor	06-28-66	205	6.1	9.9	528
3	San Fernando	Cedar Springs, Allen Ranch	02-09-71	095	6.6	86.6	813
4	San Fernando	Isabella Dam	02-09-71	014	6.6	113.0	685
5	San Fernando	Santa Felita Dam (outlet)	02-09-71	172	6.6	27.5	376
6	San Fernando	Tehachapi Pump	02-09-71	090	6.6	68.0	669
7	Friuli	Feltre	05-06-76	000	6.5	97.1	587
8	Friuli	SanRocco	09-11-76	NS	5.5	17.9	587
9	Friuli	SanRocco	09-15-76	270	6.1	12.7	587
10	Santa Barbara	Cachuma Dam Toe	08-13-78	250	6.0	36.6	438
11	Tabas	Dayhook	09-16-78	LN	7.4	17.0	587
12	Tabas	Ferdows	09-16-78	L1	7.4	94.4	587
13	Imperial Valley	Cerro Prieto	10-15-79	147	6.5	26.5	587
14	Imperial Valley	Superstition Mtn. Camera	10-15-79	045	6.5	26.0	362
15	Livermore	APEEL 3E Hayward	01-24-80	146	5.8	31.0	517
16	Livermore	APEEL 3E Hayward	01-27-80	236	5.4	31.0	517
17	Mammoth Lakes	Bishop	05-27-80	070	6.0	43.7	345
18	Victoria	Cerro Prieto	06-09-80	045	6.1	34.8	587
19	Coalinga	Parkfield Cholame 3E	05-02-83	000	6.4	38.4	376
20	Coalinga	Parkfield Stone Corral 2E	05-02-83	090	6.4	34.4	376
21	Coalinga	Parkfield Stone Corral 3E	05-02-83	090	6.4	31.8	376
22	Coalinga	Parkfield Stone Corral 4E	05-02-83	000	6.4	29.6	376
23	Coalinga	Parkfield Vineyard Cany 3W	05-02-83	020	6.4	32.3	297
24	Coalinga	Slack Canyon	05-02-83	045	6.4	27.7	685
25	Coalinga	SGT (temp)	05-09-83	080	5.0	14.1	376
26	Coalinga	VEW (temp)	05-09-83	005	5.0	12.6	376
27	Coalinga	Sulphur Baths (temp)	06-11-83	090	5.3	9.7	617
28	Coalinga	Oil Fields Fire Station	07-09-83	360	5.2	11.9	376
29	Coalinga	Oil Fields Fire Station Pad	07-09-83	270	5.2	11.9	376
30	Coalinga	Transmitter Hill	07-09-83	270	5.2	10.4	376
31	Coalinga	Oil Fields Fire Sta.	07-22-83	360	5.8	10.9	376
32	Coalinga	Oil Fields Fire Sta. Pad	07-22-83	360	5.8	10.9	376
33	Coalinga	Skunk Hollow	07-22-83	270	5.8	12.2	376
34	Coalinga	Transmitter Hill	07-22-83	270	5.8	9.2	376
35	Morgan Hill	Gilroy Array #1	04-24-84	230	6.2	16.2	1428
36	Nahanni	Site 1	12-23-85	010	6.8	6.0	587
37	Nahanni	Site 2	12-23-85	240	6.8	8.0	587
38	Nahanni	Site 3	12-23-85	270	6.8	16.0	587
39	N. Palm Springs	Whitewater Trout Farm	07-08-86	270	6.0	7.3	345
40	Chalfant Valley	Bishop Paradise Lodge	07-21-86	160	6.2	23.0	345
41	Chalfant Valley	Bishop Paradise Lodge	07-21-86 (aft)	070	5.6	14.0	345
42	Loma Prieta	Anderson Dam	10-18-89	250	6.9	21.4	392
43	Loma Prieta	APEEL 10 - Skyline	10-18-89	000	6.9	47.8	489
44	Loma Prieta	Belmont - Environtech	10-18-89	090	6.9	49.9	376
45	Loma Prieta	Berkeley LBL	10-18-89	000	6.9	83.6	628
46	Loma Prieta	BRAN	10-18-89	090	6.9	10.3	597
47	Loma Prieta	Gilroy Array #1	10-18-89	000	6.9	11.2	1428
48	Loma Prieta	Golden Gate Bridge	10-18-89	270	6.9	85.1	642
49	Loma Prieta	Hollister SAGO Vault	10-18-89	270	6.9	30.6	685
50	Loma Prieta	Los Gatos Presentation C.	10-18-89	000	6.9	6.1	466
51	Loma Prieta	Monterey City Hall	10-18-89	090	6.9	44.8	685
52	Loma Prieta	Palo Alto SLAC Lab.	10-18-89	270	6.9	36.3	425

(*continued*)

Table A1
(*Continued*)

Earthquake No.	Earthquake Name	Station Name	Date	Comp.	Mag.	Dist. (km)	$V\,s_{30}$ (m/sec)
53	Loma Prieta	Piedmont Jr. High	10-18-89	045	6.9	78.3	895
54	Loma Prieta	Point Bonita	10-18-89	207	6.9	88.6	1316
55	Loma Prieta	SF Cliff House	10-18-89	000	6.9	84.4	713
56	Loma Prieta	SF Pacific Heights	10-18-89	270	6.9	81.6	1250
57	Loma Prieta	SF Presidio	10-18-89	090	6.9	83.1	594
58	Loma Prieta	SF Rincon Hill	10-18-89	000	6.9	79.7	873
59	Loma Prieta	SF Telegraph Hill	10-18-89	090	6.9	82.0	713
60	Loma Prieta	SF Sierra Point	10-18-89	115	6.9	68.2	–
61	Loma Prieta	UCSC	10-18-89	000	6.9	17.9	714
62	Loma Prieta	Yerba Buena Island	10-18-89	090	6.9	80.6	660
63	Georgia	Ambralauri	06-15-91	X	6.2	73.7	587
64	Cape Mendocino	Cape Mendocino	04-25-92	000	7.1	8.5	539
65	Landers	Amboy	06-28-92	000	7.3	69.2	271
66	Landers	Lucerne	06-28-92	260	7.3	1.1	685
67	Landers	San Gabriel E Grand Av.	06-28-92	180	7.3	141.6	401
68	Landers	Silent Valley Poppet Flat	06-28-92	000	7.3	51.7	685
69	Landers	Twentynine Palms	06-28-92	090	7.3	42.2	685
70	Northridge	Burbank Howard Road	01-17-94	060	6.7	20.0	822
71	Northridge	LA Wonderland Av.	01-17-94	095	6.7	22.7	1223
72	Northridge	Lake Hughes #9	01-17-94	000	6.7	26.8	671
73	Northridge	Little Rock Brainard Can	01-17-94	090	6.7	46.9	822
74	Northridge	Mount Wilson CIT	01-17-94	000	6.7	36.1	822
75	Northridge	San Gabriel E Grand Av.	01-17-94	180	6.7	41.7	401
76	Northridge	Vasquez Rocks Park	01-17-94	000	6.7	24.2	996
77	Kobe	Chihaya	01-16-95	000	6.9	48.7	609
78	Kobe	Kobe University	01-16-95	090	6.9	0.2	1043

Table A2
Values of $S_a^r(f)$ and $S_a^s(f)$ for Both the Sandy and Clayey Sites

	S_a at Rock				S_a at Surface (sandy site)				S_a at Surface (clayey site)			
Eq. No.	0.33 Hz	1.0 Hz	5.0 Hz	100 Hz	0.33 Hz	1.0 Hz	5.0 Hz	100 Hz	0.33 Hz	1.0 Hz	5.0 Hz	100 Hz
1	0.1685	0.4965	0.5456	0.4759	0.4595	0.5667	0.4281	0.3282	0.3963	0.6861	0.4616	0.3117
2	0.0208	0.2059	0.5959	0.3574	0.0466	0.3982	0.5806	0.2098	0.0449	0.4858	0.7386	0.3378
3	0.0059	0.0262	0.0554	0.0198	0.0073	0.1050	0.1274	0.0413	0.0084	0.0801	0.1428	0.0772
4	0.0025	0.0057	0.0201	0.0061	0.0030	0.0255	0.0488	0.0169	0.0042	0.0197	0.0759	0.0252
5	0.0409	0.1665	0.2363	0.1484	0.0485	0.5351	0.3303	0.1532	0.0539	0.4585	0.4351	0.2054
6	0.0038	0.0067	0.1383	0.0527	0.0053	0.0244	0.3546	0.0790	0.0068	0.0376	0.3685	0.0966
7	0.0036	0.0097	0.0786	0.0326	0.0046	0.0324	0.1871	0.0536	0.0055	0.0315	0.2429	0.0690
8	0.0073	0.0148	0.0883	0.0291	0.0098	0.0554	0.2009	0.0649	0.0133	0.0535	0.2419	0.1048
9	0.0241	0.0707	0.2942	0.1344	0.0410	0.2466	0.5452	0.1906	0.0551	0.2283	0.6235	0.2679
10	0.0101	0.0732	0.1665	0.0721	0.0237	0.2747	0.2617	0.1252	0.0298	0.2417	0.4406	0.2038
11	0.0675	0.2244	1.3786	0.3279	0.0709	0.4501	0.3314	0.1911	0.1067	0.6375	1.0601	0.3210
12	0.0099	0.0329	0.2290	0.0873	0.0142	0.1310	0.3578	0.1214	0.0226	0.1179	0.5821	0.1832
13	0.0311	0.0973	0.3944	0.1691	0.0521	0.1743	0.1708	0.1409	0.0769	0.3725	0.6127	0.3255
14	0.0162	0.0261	0.2534	0.1092	0.0197	0.0837	0.5298	0.1234	0.0226	0.0901	0.6454	0.1801
15	0.0070	0.0305	0.2531	0.0722	0.0119	0.1077	0.4390	0.1173	0.0177	0.1229	0.4348	0.1931
16	0.0031	0.0121	0.0795	0.0280	0.0046	0.0587	0.1668	0.0525	0.0057	0.0444	0.2197	0.0880
17	0.0244	0.0559	0.1573	0.0906	0.0343	0.2132	0.3834	0.0994	0.0370	0.1651	0.4143	0.1224
18	0.0441	0.5947	1.0895	0.6212	0.0660	0.7860	0.2444	0.2107	0.1130	1.1733	0.6462	0.3365
19	0.0198	0.0519	0.1055	0.0437	0.0268	0.2104	0.2774	0.1086	0.0322	0.2176	0.3188	0.1756
20	0.0109	0.0845	0.1107	0.0945	0.0339	0.2383	0.2204	0.1516	0.0424	0.2980	0.3313	0.2468
21	0.0140	0.0773	0.2513	0.1057	0.0284	0.2447	0.3620	0.1391	0.0404	0.3140	0.4273	0.1697
22	0.0244	0.1043	0.1591	0.0626	0.0457	0.3128	0.2664	0.1319	0.0492	0.3499	0.3971	0.1855
23	0.0198	0.3074	0.2083	0.0985	0.0422	0.7544	0.2223	0.1806	0.0554	0.9165	0.4955	0.2854
24	0.0274	0.2483	0.2968	0.1661	0.0688	0.4783	0.3146	0.2047	0.0880	0.5803	0.3624	0.2796
25	0.0038	0.0386	0.3660	0.1389	0.0105	0.1424	0.4851	0.1300	0.0098	0.1009	0.6435	0.1788

(*continued*)

Table A2
(*Continued*)

	S_a at Rock				S_a at Surface (sandy site)				S_a at Surface (clayey site)			
Eq. No.	0.33 Hz	1.0 Hz	5.0 Hz	100 Hz	0.33 Hz	1.0 Hz	5.0 Hz	100 Hz	0.33 Hz	1.0 Hz	5.0 Hz	100 Hz
26	0.0058	0.0455	0.3135	0.1455	0.0151	0.1709	0.3018	0.1597	0.0134	0.1831	0.4823	0.1998
27	0.0247	0.0345	0.1091	0.0369	0.0339	0.1066	0.2880	0.0731	0.0438	0.1039	0.2921	0.0972
28	0.0065	0.0388	0.3100	0.0964	0.0091	0.1571	0.4048	0.1393	0.0133	0.1108	0.7142	0.2050
29	0.0040	0.0397	0.1959	0.0940	0.0081	0.1663	0.4003	0.1224	0.0086	0.1146	0.4801	0.1884
30	0.0073	0.0933	0.3943	0.2053	0.0229	0.2844	0.4244	0.2033	0.0269	0.3293	0.6105	0.2870
31	0.0314	0.1621	0.4620	0.1872	0.0653	0.4084	0.6406	0.1848	0.0706	0.5334	0.7380	0.2465
32	0.0324	0.1750	0.4867	0.2099	0.0700	0.4441	0.6784	0.1891	0.0730	0.5930	0.6976	0.2679
33	0.0396	0.1741	0.9025	0.3748	0.0769	0.4297	0.5197	0.2154	0.1002	0.5598	0.7120	0.3210
34	0.0479	0.6425	0.8631	0.8402	0.1304	0.7002	0.3455	0.2796	0.1428	0.8945	0.8032	0.3443
35	0.0052	0.0258	0.1610	0.0688	0.0085	0.1081	0.3631	0.0937	0.0130	0.0863	0.4192	0.1149
36	0.1117	0.4277	2.8188	0.9778	0.1101	0.5319	0.5147	0.2502	0.1662	0.6687	0.8461	0.3214
37	0.0404	0.1363	0.4163	0.4890	0.0693	0.3513	0.4147	0.2544	0.0783	0.5502	0.7089	0.3344
38	0.0230	0.0353	0.1765	0.1476	0.0308	0.1655	0.3876	0.1192	0.0368	0.1428	0.4805	0.1737
39	0.0236	0.3081	1.3185	0.6120	0.0497	0.4467	0.6457	0.2773	0.0540	0.4543	0.8023	0.3427
40	0.0317	0.0690	0.3524	0.1607	0.0544	0.2465	0.4410	0.1491	0.0760	0.2898	0.4539	0.2302
41	0.0038	0.0223	0.0363	0.0366	0.0052	0.0865	0.0974	0.0493	0.0061	0.0678	0.1258	0.0712
42	0.0539	0.1235	0.1102	0.0637	0.0960	0.3417	0.2356	0.1099	0.1239	0.3190	0.2912	0.1682
43	0.0729	0.1733	0.1833	0.1027	0.1097	0.3574	0.3931	0.1600	0.1446	0.4358	0.4990	0.2670
44	0.0682	0.1766	0.1804	0.1103	0.1045	0.4661	0.3111	0.1814	0.1156	0.4905	0.4899	0.2921
45	0.0112	0.1746	0.0999	0.0568	0.0321	0.4486	0.1887	0.1434	0.0315	0.4878	0.3159	0.1911
46	0.0544	0.3886	0.9361	0.5011	0.0715	0.4360	0.4260	0.2384	0.1201	0.7852	1.0728	0.3427
47	0.0485	0.1109	1.2972	0.4109	0.0848	0.2620	0.6623	0.2428	0.0987	0.3129	0.9590	0.3299
48	0.0713	0.5128	0.3373	0.2334	0.1817	0.7425	0.3315	0.3113	0.1990	0.8384	0.4589	0.3310
49	0.0157	0.0890	0.0991	0.0361	0.0213	0.3152	0.2168	0.0794	0.0275	0.2515	0.2886	0.1266
50	0.4637	1.0519	1.1930	0.5632	0.6988	0.5204	0.9159	0.5890	0.9885	0.7070	0.7797	0.3301
51	0.0104	0.0537	0.1587	0.0629	0.0182	0.1881	0.3188	0.1015	0.0207	0.2057	0.3254	0.1635
52	0.1080	0.5501	0.3774	0.1943	0.1951	0.8440	0.3627	0.2776	0.2252	1.0585	0.4720	0.3110
53	0.0189	0.0890	0.1172	0.0839	0.0346	0.2963	0.2306	0.1337	0.0466	0.3252	0.3037	0.2105
54	0.0252	0.1046	0.1578	0.0713	0.0481	0.2742	0.2673	0.1266	0.0567	0.2686	0.3554	0.2161
55	0.0268	0.1515	0.1271	0.0745	0.0398	0.4141	0.2486	0.1711	0.0520	0.4511	0.3130	0.2378
56	0.0419	0.1311	0.0821	0.0609	0.0648	0.3439	0.1606	0.1234	0.0869	0.3696	0.2309	0.1532
57	0.0649	0.2899	0.3751	0.1999	0.1503	0.5929	0.3769	0.2880	0.1763	0.6634	0.3975	0.3111
58	0.0181	0.1174	0.1506	0.0784	0.0324	0.3904	0.1672	0.0995	0.0464	0.3617	0.4314	0.1602
59	0.0142	0.0938	0.1459	0.0768	0.0263	0.3078	0.2595	0.1482	0.0284	0.3213	0.2384	0.2004
60	0.0232	0.0784	0.1230	0.0560	0.0352	0.2800	0.2253	0.1060	0.0398	0.2567	0.2830	0.1825
61	0.0204	0.2969	1.4216	0.4502	0.0406	0.7489	0.7391	0.5530	0.0514	0.9133	0.8854	0.3304
62	0.0334	0.0734	0.1007	0.0678	0.0533	0.2271	0.2026	0.1256	0.0727	0.3355	0.2770	0.2478
63	0.0038	0.0294	0.0345	0.0177	0.0054	0.1121	0.0878	0.0462	0.0092	0.1112	0.1147	0.0635
64	0.1896	0.7508	2.6993	1.4973	0.2236	0.8064	0.5695	0.3089	0.2988	0.7953	1.3840	0.3717
65	0.0865	0.1866	0.3022	0.1150	0.1291	0.5482	0.4985	0.1578	0.1511	0.5304	0.6788	0.2100
66	0.3264	0.4772	1.2578	0.7268	0.3764	0.5500	0.5527	0.3755	0.4899	0.6709	1.0546	0.3303
67	0.0346	0.0924	0.0642	0.0410	0.0459	0.2727	0.1477	0.0998	0.0656	0.2608	0.1922	0.1491
68	0.0169	0.0254	0.1032	0.0499	0.0200	0.1097	0.2375	0.0810	0.0256	0.0790	0.2770	0.0906
69	0.0213	0.0290	0.1688	0.0603	0.0236	0.1278	0.3334	0.0974	0.0271	0.1059	0.4745	0.1244
70	0.0215	0.0898	0.3428	0.1197	0.0314	0.3013	0.3960	0.1747	0.0338	0.2945	0.5667	0.2808
71	0.0132	0.1006	0.2717	0.1123	0.0366	0.2934	0.4219	0.1489	0.0366	0.3602	0.5148	0.2175
72	0.0130	0.0315	0.6461	0.1652	0.0219	0.1228	0.8629	0.1804	0.0318	0.1358	1.0548	0.2699
73	0.0112	0.1473	0.2201	0.0720	0.0165	0.4463	0.2379	0.1256	0.0181	0.4482	0.4169	0.1781
74	0.0066	0.0576	0.8351	0.2339	0.0149	0.2796	0.7513	0.1699	0.0169	0.2582	1.0365	0.3308
75	0.0199	0.1475	0.6104	0.2560	0.0337	0.5096	0.8381	0.2027	0.0375	0.5486	0.8995	0.3080
76	0.0286	0.1917	0.2705	0.1510	0.0873	0.5131	0.4101	0.2023	0.1098	0.5074	0.7402	0.2720
77	0.0096	0.0567	0.2126	0.0933	0.0144	0.1803	0.4110	0.1255	0.0156	0.1807	0.5695	0.2342
78	0.0928	0.3853	0.4278	0.3105	0.1624	0.7732	0.3894	0.2493	0.1755	0.9456	0.5851	0.3083

Geodeco S.p.A.
Via Aurelia 24
16031 Bogiasco (GE)
Italy
paolo@stanfordalumni.org
(P.B.)

Civil and Environmental Engineering Department
Stanford University
Stanford, California 94305
(C.A.C.)

Manuscript received 10 September 2003.